

## SUPPORTING INFORMATION

### **Fluorinated Dibenzo[*a,c*]-phenazine-Based Green to Red Thermally Activated Delayed Fluorescent OLED Emitters**

Gloria Hong,<sup>a†</sup> Changfeng Si,<sup>b†</sup> Abhishek Kumar Gupta,<sup>b,c†</sup> Claudia Bizzarri,<sup>a</sup> Martin Nieger,<sup>d</sup>  
Ifor D. W. Samuel,<sup>c\*</sup> Eli Zysman-Colman,<sup>b\*</sup> Stefan Bräse<sup>\*a,e</sup>

<sup>a</sup> Institute of Organic Chemistry, Karlsruhe Institute of Technology (KIT), Fritz-Haber-Weg 6, 76131  
Karlsruhe, Germany

<sup>b</sup> Organic Semiconductor Centre, EaStCHEM School of Chemistry, University of St Andrews, St  
Andrews, Fife, UK. KY16 9ST, Fax: +44-1334 463808; Tel: +44-1334 463826

<sup>c</sup> Organic Semiconductor Centre, SUPA School of Physics and Astronomy, University of St Andrews,  
St Andrews, Fife, UK. KY16 9SS, Fax: +44-1334 463808; Tel: +44-1334 463826

<sup>d</sup> M. Nieger Department of Chemistry, University of Helsinki, P. O. Box 55, 00014 University of Helsinki,  
Finland.

<sup>e</sup> Institute of Biological and Chemical Systems (IBCS-FMS), Karlsruhe Institute of Technology (KIT),  
Hermann-von-Helmholtz-Platz 1, 76344 Eggenstein-Leopoldshafen, Germany

Corresponding: braese@kit.edu, eli.zysman-colman@st-andrews.ac.uk, idws@st-andrews.ac.uk;

Keywords: thermally activated delayed fluorescence, OLED, dibenzo[*a,c*]phenazine

## Contents

<b>1. General Methods</b> .....	<b>S3</b>
1.1. General Information on Analysis Methods and Synthesis .....	S3
1.2. Theoretical Calculation .....	S4
1.3. Photophysical Measurements .....	S4
1.4. Electrochemical Measurements .....	S6
<b>2. Synthesis</b> .....	<b>S7</b>
2.1. Synthesis Procedures .....	S7
2.2. NMR Spectra .....	S12
<b>3. Crystal Structure Determinations</b> .....	<b>S18</b>
<b>4. DFT Calculations</b> .....	<b>S20</b>
<b>5. Photophysical Properties</b> .....	<b>S24</b>
<b>6. OLED Fabrication and Characterization</b> .....	<b>S29</b>
<b>7. References</b> .....	<b>S33</b>

## 1. General Methods

### 1.1. General Information on Analysis Methods and Synthesis

#### *<sup>1</sup>H Nuclear Magnetic Resonance Spectroscopy (NMR)*

<sup>1</sup>H NMR spectra were recorded on BRUKER Avance 400 (400 MHz) and BRUKER Avance DRX 500 (500 MHz) spectrometers. Chemical shifts are given in parts per million ( $\delta$ /ppm), downfield from tetramethylsilane (TMS), and are referenced to chloroform (7.26 ppm) or benzene (7.16 ppm) as internal standard. All coupling constants are absolute values, and  $J$  values are expressed in Hertz (Hz). The description of signals includes: s = singlet, bs = broad singlet, d = doublet, t = triplet, dd = doublet of doublets, ddd = doublet of doublet of doublets, dt = doublet of triplets, q = quartet, quin = quintet, sxt = sextet, sept = septet, m = multiplet. The spectra were analyzed according to the first order. <sup>13</sup>C NMR spectra were recorded on BRUKER Avance 400 (100 MHz) and BRUKER Avance DRX 500 (125 MHz) spectrometers. Chemical shifts are expressed in parts per million ( $\delta$ /ppm) downfield from tetramethylsilane (TMS) and are referenced to chloroform (77.16 ppm) or benzene (128.06 ppm) as internal standard. <sup>19</sup>F NMR spectra were recorded on BRUKER Avance 400 (376 MHz). Chemical shifts are stated in parts per million ( $\delta$ /ppm).

#### *Mass Spectrometry (MS)*

Electron ionization (EI) and fast atom bombardment (FAB) experiments were conducted using a Finnigan MAT 90 (70 eV) instrument, with 3-nitrobenzyl alcohol (3-NBA) as matrix and reference for high resolution. For the interpretation of the spectra, molecular peaks [M]<sup>+</sup>, peaks of protonated molecules [M+H]<sup>+</sup>, and characteristic fragment peaks are indicated with their mass-to-charge ratio ( $m/z$ ), and in the case of EI, their intensity in percent, relative to the base peak (100%) is given. In the case of high-resolution measurements, the tolerated error is 0.0005  $m/z$ .

#### *Infrared Spectroscopy (IR)*

The infrared spectra were recorded with a Bruker, Alpha P instrument. All samples were measured by attenuated total reflection (ATR). The positions of the absorption bands are given in wavenumbers  $\bar{\nu}$  in  $\text{cm}^{-1}$  and were measured in the range from  $3600 \text{ cm}^{-1}$  to  $500 \text{ cm}^{-1}$ . Characterization of the absorption bands was done in dependence of the transmission strength with the following abbreviations: vs (very strong, 100–90%), s (strong, 89–70%), m (medium, 59–40%), w (weak, 39–10%), vw (very weak, 0–9%).

### *Reaction Monitoring*

Routine monitoring of reactions was performed using silica gel coated aluminum plates (Merck, silica gel 60, F254) which were analyzed under UV-light at 254 nm and 365 nm. Solvent mixtures are understood as v/v.

### *Materials and Methods*

Solvents, reagents, and chemicals were purchased from abcr, Fluorochem, Sigma Aldrich and used without further purification. Air- and moisture-sensitive reactions were carried out under argon atmosphere in sealable vials using standard Schlenk techniques. Liquids were added with a stainless-steel cannula, and solids were added in powdered shape. Solvents were evaporated under reduced pressure at 45 °C using a rotary evaporator. For solvent mixtures, each solvent was measured volumetrically. Flash column chromatography was performed using Merck silica gel 60 (0.040 × 0.063 mm, 230–400 mesh ASTM) and quartz sand (glowed and purified with hydrochloric acid).

## **1.2. Theoretical Calculation**

Density functional theoretical (DFT) calculation and time-dependent density functional theoretical (TDDFT) calculations were performed using Gaussian 09 Revision D.01 software<sup>1</sup> in the gas phase. The ground state geometries were optimized employing the PBE0<sup>2</sup> functional with the Pople 6-31G(d,p) basis set,<sup>3</sup> in the gas phase. Transitions to excited singlet and triplet states were calculated using TDDFT within the Tamm-Dancoff approximation (TDA) based on the optimized ground-state geometries.<sup>4</sup>

## **1.3. Photophysical Measurements**

All samples were prepared in HPLC grade toluene (PhMe), dichloromethane (DCM), or acetonitrile (MeCN) with varying concentrations on the order of 10<sup>-5</sup> or 10<sup>-6</sup> M for absorption and emission study. Absorption spectra were recorded at RT using a Shimadzu UV-2600 double beam spectrophotometer. Molar absorptivity determination was verified by linear least-squares fit of values obtained from at least five independent solutions at varying concentrations with absorbance ranging from 6.50 × 10<sup>-5</sup> to 3.4 × 10<sup>-2</sup> M<sup>-1</sup> cm<sup>-1</sup> for **2DTCz-BP-F**, 2.04 × 10<sup>-5</sup> to 1.2 × 10<sup>-2</sup> M<sup>-1</sup> cm<sup>-1</sup> for **2DMAC-BP-F**, 3.10 × 10<sup>-5</sup> to 1.91 × 10<sup>-2</sup> M<sup>-1</sup> cm<sup>-1</sup> for **2PXZ-BP-F**. Degassed solutions were prepared via three freeze-pump-thaw cycles before emission analysis using an in-house adapted fluorescence cuvette; itself purchased from Starna. Steady-state emission and time-resolved emission spectra were recorded at 298 K using an Edinburgh Instruments F980 fluorimeter. All the samples for the steady-state measurements were excited

at 350 nm using a Xenon lamp, while the samples for the time-resolved measurements were excited at 378 nm using a picosecond laser (PicoQuant, LDH-D-C-375) driven by a laser driver (PDL 800-D). The short-time range (500 ns – 20  $\mu$ s) of PL decays were measured using time-correlated single-photon counting (TCSPC) mode. The long-time range (200  $\mu$ s – 200 ms) of PL decays were measured using multi-channel scaling (MCS) mode. In MCS mode, the picosecond laser was triggered by a delay generator (Stanford Research Systems, DG645) in burst mode. The burst mode increased the excitation pulse duration to increase the excitation power to speed up the measurement.

Photoluminescence quantum yields for solutions were excited at 360 nm for **2DTCz-BP-F**, **2DMAC-BP-F**, and **2PXZ-BP-F** and determined using the optically dilute method.<sup>5, 6</sup> The Beer-Lambert law was found to be linear at the concentrations of the solutions. For each sample, linearity between absorption and emission intensity was verified through linear regression analysis, and additional measurements were acquired until the Pearson regression factor ( $R^2$ ) for the linear fit of the data set surpassed 0.9. Individual relative quantum yield values were calculated for each solution, and the values reported represent the gradient value. The equation  $\Phi_s = \Phi_r(A_r/A_s)(I_s/I_r)(n_s/n_r)^2$  was used to calculate the relative quantum yield of each of the samples, where  $\Phi_r$  is the absolute quantum yield of the reference,  $n$  is the refractive index of the solvent,  $A$  is the absorbance at the excitation wavelength, and  $I$  is the integrated area under the corrected emission curve. The subscripts  $s$  and  $r$  refer to the sample and reference, respectively. A solution of Rhodamine 6G ( $\Phi_r = 94\%$  in ethanol)<sup>7</sup> was used as the external reference. A Hamamatsu C9920-02 integrating sphere was employed for  $\Phi_{PL}$  measurements for thin-film samples. A xenon lamp coupled to a monochromator enabled selective excitation, chosen here to be 300 nm. The output was then fed into the integrating sphere via a fiber, exciting the sample. PL spectra were collected with multimode fiber and detected with a back-thinned CCD. Doped thin films were prepared by mixing 10 wt% sample and PMMA or varying concentrations of emitter and mCP or mCBP in chloroform solution, followed by spin-coating on a quartz substrate. The quantum yields of the films were measured in air and  $N_2$  atmosphere by purging the integrating sphere with flowing  $N_2$  gas.

The singlet-triplet splitting energy,  $\Delta E_{ST}$ , was estimated by recording the prompt fluorescence, and the delayed phosphorescence spectra at 77 K. 77 K glass samples were prepared by transferring 2-MeTHF solution into NMR tubes. The NMR tubes were cooled down inside a suprasil nitrogen dewar flask by liquid nitrogen. Glass samples were photoexcited using a femtosecond laser emitting at 343 nm (Orpheus-N, model: PN13F1). Emission from the samples was focused onto a spectrograph (Chromex 250is Imaging Spectrograph) and detected with a sensitive gated iCCD camera (Stanford Computer Optics, 4Picos) having sub-

nanosecond resolution. Prompt fluorescence spectra were integrated by iCDD between 1 ns – 100 ns after the laser excitation. Phosphorescence spectra were integrated by iCDD between 1– 8.5 ms after the laser excitation for the solution. The energy values of the lowest singlet and triplet states were determined from the onset of fluorescence and phosphorescence spectra at 77 K, respectively.

#### 1.4. Electrochemical Measurements

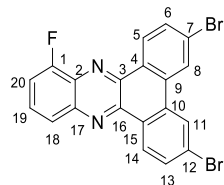
Cyclic voltammetry experiments were performed with a Gamry Interface 1010B in a three electrodes electrochemical cell. The electrochemical cell was equipped with a glassy carbon (GC) working electrode, Ag/AgNO<sub>3</sub> reference electrode, and a Pt wire as the auxiliary electrode. All the experiments were performed in dichloromethane (0.1 M TBAPF<sub>6</sub>) solution, under Ar atmosphere, whereas the concentration of the investigated compounds was 2 mM. Ferrocene (Fc) was added after each experiment as an internal standard, according to the IUPAC recommendation.<sup>8</sup> The redox properties are reported versus SCE couple according to the following equation:<sup>9</sup>

$$E_{\text{ox/red}} [\text{V vs. SCE}] = E_{\text{ox/red}} [\text{V vs. Fc/Fc}^+] + 0.46$$

## 2. Synthesis

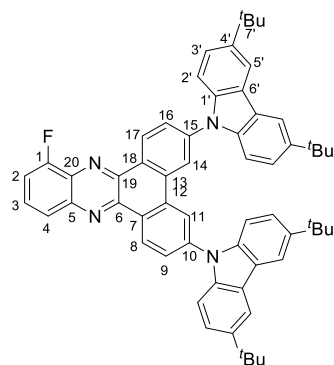
### 2.1. Synthesis Procedures

#### 3,6-dibromo-10-fluorodibenzo[*a,c*]phenazine (2Br-BP-F) (3)



A sealable vial is charged with 3-fluorobenzene-1,2-diamine (800 mg, 6.34 mmol, 1.00 equiv.) and 3,6-dibromophenanthrene-9,10-dione (2.32 g, 6.34 mmol, 1.00 equiv.). Then, acetic acid (10.7 mL, 96%) and ethanol (2.67 mL) are added and the reaction stirred at 100 °C for 21 h. Subsequently, the precipitate is filtered off and dried under reduced pressure to give 3,6-dibromo-10-fluorodibenzo[*a,c*]phenazine (2.65 g, 92%) as a beige solid.  $^{19}\text{F}$  NMR (376 MHz,  $\text{C}_6\text{D}_6$ )  $\delta$  = -123.92.  $^1\text{H}$  NMR (400 MHz, Benzene- $d_6$ )  $\delta$  = 9.22 (d,  $^3J_{\text{H,H}}$  = 8.6 Hz, 1H, 14-H), 9.12 (d,  $^3J_{\text{H,H}}$  = 8.5 Hz, 1H, 5-H), 8.15 (dd,  $J$  = 4.6 Hz,  $^4J_{\text{H,H}}$  = 1.9 Hz, 2H, 8-H, 11-H), 7.94 (d,  $^3J_{\text{H,H}}$  = 8.4 Hz, 1H, 18-H), 7.53 (ddd,  $^3J_{\text{H,H}}$  = 8.2 Hz,  $J$  = 5.7 Hz,  $^4J_{\text{H,H}}$  = 1.9 Hz, 2H, 6-H, 13-H), 7.11 (dd,  $^3J_{\text{H,H}}$  = 8.1 Hz,  $^4J_{\text{H,F}}$  = 5.5 Hz, 1H, 19-H), 7.04–6.97 (m, 1H, 20-H). IR (ATR,  $\tilde{\nu}$ ) = 1931 (vw), 1628 (w), 1595 (m), 1567 (w), 1537 (m), 1493 (m), 1485 (m), 1395 (m), 1358 (m), 1347 (vs), 1329 (w), 1248 (m), 1140 (m), 1098 (vs), 1088 (s), 1064 (m), 1028 (m), 867 (m), 839 (s), 820 (vs), 786 (m), 754 (vs), 711 (m), 591 (m), 551 (vs), 537 (s), 467 (w)  $\text{cm}^{-1}$ . HRMS–EI ( $m/z$ ): Found 453.9110. Calc. for  $[\text{C}_{20}\text{H}_9\text{N}_2^{79}\text{Br}_2\text{F}]^+$ : 453.9111. EA: Found C 52.55; H 1.80; N 6.14. Calc. for  $\text{C}_{20}\text{H}_9\text{Br}_2\text{FN}_2$ : C 52.67; H 1.99; N 6.14%. M.p.: 305 °C.

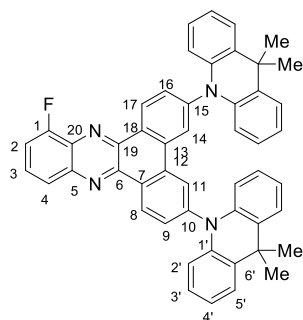
#### 3,6-bis(3,6-di-*tert*-butyl-9*H*-carbazol-9-yl)-10-fluorodibenzo[*a,c*]phenazine (4)



To a sealable vial, 3,6-dibromo-10-fluorodibenzo[*a,c*]phenazine (1.00 g, 2.19 mmol, 1.00 equiv.), 3,6-di-*tert*-butyl-9*H*-carbazole (1.23 g, 4.38 mmol, 2.00 equiv.), NaOtBu (632 mg, 6.58 mmol, 3.00 equiv.), Pd(OAc)<sub>2</sub> (49.2 mg, 219  $\mu\text{mol}$ , 0.100 equiv.) were added and the vial was evacuated and backfilled with argon. Then, toluene (10.0 mL, abs.) was added and P(*t*Bu)<sub>3</sub>

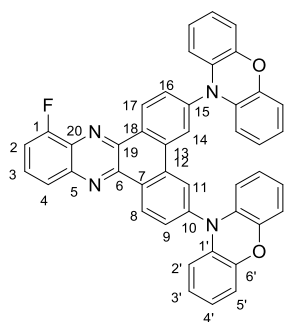
(88.7 mg, 438  $\mu$ L, 438  $\mu$ mol, 1.00M in toluene, 0.200 equiv.) was added dropwise. Subsequently, the solution was stirred at 110  $^{\circ}$ C until TLC indicates full consumption of the starting material after 18 h. Then, the product mixture was cooled to room temperature and pulled over a Celite plug with dichloromethane. The filtrate was concentrated under reduced pressure. The crude product was purified *via* column chromatography (cyclohexane:dichloromethane = 5:1  $\rightarrow$  2:1). 3,6-bis(3,6-di-*tert*-butyl-9*H*-carbazol-9-yl)-10-fluorodibenzo[*a,c*]phenazine (1.81 g, 97%) was obtained as a bright orange-yellow solid.  $^{19}\text{F}$  NMR (376 MHz,  $\text{CDCl}_3$ )  $\delta$  = -124.46;  $^1\text{H}$  NMR (400 MHz, Chloroform-*d*)  $\delta$  = 9.60 (d,  $^3J_{\text{H,H}}$  = 8.6 Hz, 1H, 8-H), 9.54 (d,  $^3J_{\text{H,H}}$  = 8.6 Hz, 1H, 17-H), 8.66 (dd,  $J$  = 3.1,  $^4J_{\text{H,H}}$  = 2.0 Hz, 2H, 11-H, 14-H), 8.17 (d,  $^4J_{\text{H,H}}$  = 1.9 Hz, 4H, 5'-H), 8.13 (dd,  $^3J_{\text{H,H}}$  = 8.6 Hz,  $^4J_{\text{H,H}}$  = 1.2 Hz, 1H, 4-H), 8.01 (ddd,  $^3J_{\text{H,H}}$  = 8.6 Hz,  $^4J_{\text{H,H}}$  = 3.2 Hz,  $^4J_{\text{H,H}}$  = 1.9 Hz, 2H, 9-H, 16-H), 7.81 (ddd,  $^3J_{\text{H,H}}$  = 8.6 Hz,  $^3J_{\text{H,H}}$  = 7.7 Hz,  $^4J_{\text{H,F}}$  = 5.4 Hz, 1H, 3-H), 7.59–7.51 (m, 5H, 2-H, 2'-H), 7.43 (ddd,  $^3J_{\text{H,H}}$  = 8.7 Hz,  $^4J_{\text{H,H}}$  = 3.6 Hz,  $^4J_{\text{H,H}}$  = 1.9 Hz, 4H, 3'-H), 1.47 (s, 18H,  $\text{CH}_3$ ), 1.46 (s, 18H,  $\text{CH}_3$ ).  $^{13}\text{C}$  NMR (101 MHz,  $\text{CDCl}_3$ )  $\delta$  = 157.59 (d,  $^1J_{\text{C,F}}$  = 261.8 Hz), 143.70 (2C, C-4'), 143.67 (2C, C-4'), 143.18 (C-10), 142.57 (C-15), 141.80 (d,  $^3J_{\text{C,F}}$  = 2.12 Hz, C-5), 140.96 (C-12), 140.92 (C-13), 138.87 (4C, C-1'), 133.36 (C-6), 133.28 (d,  $^2J_{\text{C,F}}$  = 12.2 Hz, C-20), 133.15 (C-19), 129.26 (d,  $^3J_{\text{C,F}}$  = 8.3 Hz, C-3), 128.84 (C-8), 128.58 (C-7), 128.55 (C-18), 128.46 (C-17), 126.67 (C-9), 126.56 (C-16), 125.40 (d,  $^4J_{\text{C,F}}$  = 4.4 Hz, C-4), 124.17 (4C, 2'), 123.97 (4C, C-6'), 120.27 (C-11), 120.19 (C-14), 116.57 (4C, C-5'), 113.62 (d,  $^2J_{\text{C,F}}$  = 18.2 Hz, C-2), 109.27 (4C, C-2'), 34.90 (4C,  $\text{C}_q$ ), 32.11 (12C,  $\text{CH}_3$ ). **MS** (FAB, 3-NBA),  $m/z$  (%): 856 (27), 855 (69), 854 (100), 853 (75), 852 (30), 839 (29), 838 (40), 797 (25). **HRMS–FAB** ( $m/z$ ): Found 853.4641. Calc. for  $[\text{C}_{60}\text{H}_{58}\text{N}_4\text{F}]^+$ : 853.4640. **IR** (ATR,  $\tilde{\nu}$ ) = 3053 (vw), 2951 (s), 2928 (m), 2901 (m), 2864 (m), 1606 (vs), 1572 (w), 1543 (w), 1513 (m), 1489 (vs), 1473 (vs), 1452 (vs), 1394 (m), 1363 (vs), 1322 (vs), 1295 (vs), 1259 (vs), 1228 (vs), 1201 (m), 1180 (m), 1146 (m), 1092 (vs), 1033 (m), 877 (s), 841 (m), 807 (vs), 793 (s), 752 (s), 738 (vs), 717 (m), 650 (m), 608 (vs), 561 (m), 469 (m), 421 (s)  $\text{cm}^{-1}$ . **EA**: Found C 84.35; H 6.87; N 6.44. Calc. for  $\text{C}_{60}\text{H}_{57}\text{FN}_4$ : C 84.47; H 6.73; N 6.57%. **R<sub>f</sub>** = 0.66 (cyclohexane:ethyl acetate=50:1). **M.p.**: 266  $^{\circ}$ C.

### 3,6-bis(9,9-dimethylacridin-10(9*H*)-yl)-10-fluorodibenzo[*a,c*]phenazine (5)



A sealable vial was charged with 3,6-dibromo-10-fluorodibenzo[*a,c*]phenazine (700 mg, 1.53 mmol, 1.00 equiv.), 9,9-dimethyl-10*H*-acridine (642 mg, 3.07 mmol, 2.00 equiv.), P(*t*Bu)<sub>3</sub> (62.1 mg, 307 μL, 307 μmol, 1.00M in toluene, 0.200 equiv.), NaO*t*Bu (442 mg, 4.60 mmol, 3.00 equiv.) and Pd(OAc)<sub>2</sub> (34.5 mg, 153 μmol, 0.100 equiv.). Then, the vial was sealed and evacuated and backfilled with argon three times. Subsequently, toluene (15.0 mL, abs.) was added and the solution was heated at 120 °C for 18 h. Then, the product mixture was cooled to room temperature and pulled over a Celite plug with dichloromethane. The filtrate was concentrated under reduced pressure. The crude product was purified *via* column chromatography (cyclohexane:dichloromethane = 5:1 → 4:1). 3,6-Bis(9,9-dimethylacridin-10(9*H*)-yl)-10-fluorodibenzo[*a,c*]phenazine (0.897 g, 82%) was obtained as an orange solid. <sup>19</sup>F NMR (376 MHz, CDCl<sub>3</sub>) δ = -124.37. <sup>1</sup>H NMR (500 MHz, Methylene Chloride-*d*<sub>2</sub>) δ = 9.73 (d, <sup>3</sup>J<sub>H,H</sub> = 8.5 Hz, 1H, 8-H), 9.71 (d, <sup>3</sup>J<sub>H,H</sub> = 8.5 Hz, 1H, 17-H), 8.48 (t, <sup>4</sup>J<sub>H,H</sub> = 2.5 Hz, 2H, 11-H, 14-H), 8.23 (dt, <sup>3</sup>J<sub>H,H</sub> = 8.5 Hz, <sup>4</sup>J<sub>H,H</sub> = 1.1 Hz, 1H, 4-H), 7.89 (ddd, <sup>3</sup>J<sub>H,H</sub> = 8.7 Hz, <sup>3</sup>J<sub>H,H</sub> = 7.8 Hz, <sup>3</sup>J<sub>H,F</sub> = 5.4 Hz, 1H, 3-H), 7.78 (ddd, <sup>3</sup>J<sub>H,H</sub> = 8.5 Hz, <sup>4</sup>J<sub>H,H</sub> = 2.5 Hz, 2H, 9-H, 16-H), 7.63 (ddd, <sup>3</sup>J<sub>C,F</sub> = 10.0 Hz, <sup>3</sup>J<sub>H,H</sub> = 7.8 Hz, <sup>4</sup>J<sub>H,H</sub> = 1.1 Hz, 1H, 2-H), 7.50–7.44 (m, 4H, 5'-H), 6.98–6.86 (m, 8H, 3'-H, 4'-H), 6.41–6.31 (m, 4H, 2'-H), 1.69 (s, 12H, CH<sub>3</sub>). <sup>13</sup>C NMR (126 MHz, CD<sub>2</sub>Cl<sub>2</sub>) δ = 157.88 (d, <sup>1</sup>J<sub>C,F</sub> = 261.1 Hz, C-1), 144.40 (C-10), 144.35 (C-15), 143.70 (C-6), 143.11 (C-18), 142.27 (d, <sup>3</sup>J<sub>C,F</sub> = 2.29 Hz, C-5), 141.07 (4C, C-1'), 134.91 (C-12), 134.76 (C-13), 133.75 (d, <sup>2</sup>J<sub>C,F</sub> = 12.36 Hz, C-20), 132.20 (C-9), 132.11 (C-16), 130.59 (2C, C-6'), 130.57 (2C, C-6'), 130.34 (C-7), 130.24 (C-18), 130.00 (d, <sup>3</sup>J<sub>C,F</sub> = 8.14 Hz, C-3), 129.95 (C-8), 129.82 (C-17), 126.79 (4C, C-4'), 126.67 (C-11), 126.63 (C-14), 125.85 (4C, 5'), 125.80 (d, <sup>5</sup>J<sub>C,F</sub> = 4.57 Hz, C-4), 121.20 (2C, C-3'), 121.19 (2C, C-3'), 114.51 (4C, C-2'), 114.16 (d, <sup>2</sup>J<sub>C,F</sub> = 18.28 Hz, C-2), 36.35 (2C, C<sub>q</sub>), 31.72 (4C, CH<sub>3</sub>). MS (FAB, 3-NBA), *m/z* (%): 714 (42), 713 (77), 712 (42), 698 (55), 697 (100), 154 (99), 137 (61), 136 (80), 95 (42). HRMS–FAB (*m/z*): Found 713.3077. Calc. for [C<sub>50</sub>H<sub>38</sub>N<sub>4</sub>F]<sup>+</sup>: 713.3075. IR (ATR,  $\tilde{\nu}$ ) = 3072 (w), 3048 (w), 3040 (w), 2965 (w), 2918 (w), 2857 (w), 1589 (s), 1502 (w), 1480 (s), 1465 (s), 1443 (vs), 1356 (s), 1330 (vs), 1286 (s), 1265 (vs), 1247 (s), 1218 (m), 1205 (w), 1089 (s), 1061 (w), 1047 (m), 931 (w), 849 (w), 741 (vs), 728 (vs), 698 (s), 681 (m), 642 (vs), 568 (m), 523 (m), 487 (m) cm<sup>-1</sup>. EA: Found C 84.04; H 5.12; N 7.84. Calc. for C<sub>50</sub>H<sub>37</sub>N<sub>4</sub>: C 84.24; H 5.23; N 7.86%. R<sub>f</sub> = 0.59 (cyclohexane:ethyl acetate = 4:1). M.p.: 362 °C.

### 10,10'-(10-fluorodibenzo[*a,c*]phenazine-3,6-diyl)bis(10*H*-phenoxazine) (6)



A sealable vial was charged with 3,6-dibromo-10-fluorodibenzo[*a,c*]phenazine (651 mg, 1.43 mmol, 1.00 equiv.), 10*H*-phenoxazine (575 mg, 3.14 mmol, 2.20 equiv.), TTBP · HBF<sub>4</sub> (50.1 mg, 173 μmol, 0.121 equiv.), NaOtBu (412 mg, 4.28 mmol, 3.00 equiv.) and Pd(dba)<sub>2</sub> (47.0 mg, 81.7 μmol, 0.0573 equiv.). It was then sealed and evacuated and backfilled with argon. Then, toluene (15.2 mL, abs.) was added. The reaction mixture was stirred at 120 °C for 14 h. The product mixture was pulled over a Celite plug with dichloromethane and the filtrate was concentrated under reduced pressure. The crude product was purified by means of column chromatography (cyclohexane:dichloromethane = 4:1). 10,10'-(10-Fluorodibenzo[*a,c*]phenazine-3,6-diyl)bis(10*H*-phenoxazine) (943 mg, quant.) was obtained as a bright red solid. <sup>19</sup>F NMR (376 MHz, CDCl<sub>3</sub>) δ = -124.28. <sup>1</sup>H NMR (500 MHz, Chloroform-*d*) δ = 9.72 (d, <sup>3</sup>J<sub>H,H</sub> = 8.5 Hz, 1H, 8-H), 9.67 (d, <sup>3</sup>J<sub>H,H</sub> = 8.5 Hz, 1H, 17-H), 8.49 (dd, *J* = 4.0 Hz, <sup>4</sup>J<sub>H,H</sub> = 1.9 Hz, 2H, 11-H, 14-H), 8.21 (dt, <sup>3</sup>J<sub>H,H</sub> = 8.6 Hz, <sup>4</sup>J<sub>H,H</sub> = 1.0 Hz, 1H, 4-H), 7.87 (ddd, <sup>3</sup>J<sub>H,H</sub> = 8.6 Hz, <sup>3</sup>J<sub>H,H</sub> = 7.7 Hz, <sup>4</sup>J<sub>H,F</sub> = 5.4 Hz, 1H, 3-H), 7.79 (dt, <sup>3</sup>J<sub>H,H</sub> = 8.4 Hz, <sup>4</sup>J<sub>H,H</sub> = 2.2 Hz, 2H, 9-H, 16-H), 7.61 (ddd, <sup>3</sup>J<sub>H,F</sub> = 9.1 Hz, <sup>3</sup>J<sub>H,H</sub> = 7.7 Hz, <sup>4</sup>J<sub>H,H</sub> = 1.2 Hz, 1H, 2-H), 6.73 (dt, <sup>3</sup>J<sub>H,H</sub> = 7.8 Hz, <sup>4</sup>J<sub>H,H</sub> = 1.2 Hz, 4H, 5'-H), 6.70–6.64 (m, 4H, 4'H), 6.58 (td, <sup>3</sup>J<sub>H,H</sub> = 7.7 Hz, <sup>4</sup>J<sub>H,H</sub> = 1.5 Hz, 4H, 3'-H), 6.03 (dt, <sup>3</sup>J<sub>H,H</sub> = 8.1 Hz, <sup>4</sup>J<sub>H,H</sub> = 1.5 Hz, 4H, 2'-H). <sup>13</sup>C NMR (126 MHz, CDCl<sub>3</sub>) δ = 157.63 (d, <sup>1</sup>J<sub>C,F</sub> = 262.2 Hz, C-1), 144.13 (4C, C-6'), 143.39 (C-6), 142.62 (C-19), 141.87 (C-10), 141.83 (d, <sup>3</sup>J<sub>C,F</sub> = 2.4 Hz, C-5), 141.79 (C-15), 134.47 (C-17), 134.27 (C-13), 134.17 (2C, C-1'), 134.16 (2C, C-1'), 133.57 (d, <sup>2</sup>J<sub>C,F</sub> = 12.5 Hz, C-20), 131.42 (C-9), 131.32 (C-16), 130.23 (C-7), 130.21 (C-8), 130.13 (C-18), 129.96 (C-17), 129.79 (d, <sup>3</sup>J<sub>C,F</sub> = 8.3 Hz, C-3), 126.04 (C-11), 125.93 (C-14), 125.56 (d, <sup>4</sup>J<sub>C,F</sub> = 4.6 Hz, C-4), 123.48 (4C, C-3'), 121.94 (2C, C-4'), 121.92 (2C, C-4'), 115.86 (4C, C-5'), 114.03 (d, <sup>2</sup>J<sub>C,F</sub> = 18.2 Hz, C-2), 113.44 (2C, C-22), 113.43 (2C, C-22). MS (ESI), *m/z* (%): 663 (100), 662 (65), 647 (56), 154 (43). HRMS–FAB (*m/z*): Found 660.1956. Calc. for [C<sub>44</sub>H<sub>25</sub>O<sub>2</sub>N<sub>4</sub>F]<sup>+</sup>: 660.1956. IR (ATR,  $\tilde{\nu}$ ) = 3060 (w), 1625 (w), 1602 (m), 1592 (w), 1506 (w), 1485 (vs), 1463 (m), 1402 (w), 1354 (s), 1332 (vs), 1292 (m), 1272 (vs), 1252 (s), 1224 (w), 1200 (m), 1128 (w), 1091 (m), 1043 (m), 936 (w), 866 (w), 752 (m), 739 (vs), 728 (vs), 632 (s), 446 (w) cm<sup>-1</sup>. EA: Found C 80.15; H 3.75; N 8.35. Calc.

for (C<sub>44</sub>H<sub>25</sub>FN<sub>4</sub>O<sub>2</sub>): C 79.99; H 3.81; N 8.48%. **R<sub>f</sub>** = 0.76 (cyclohexane:ethyl acetate = 4:1).  
**M.p.**: 315 °C.



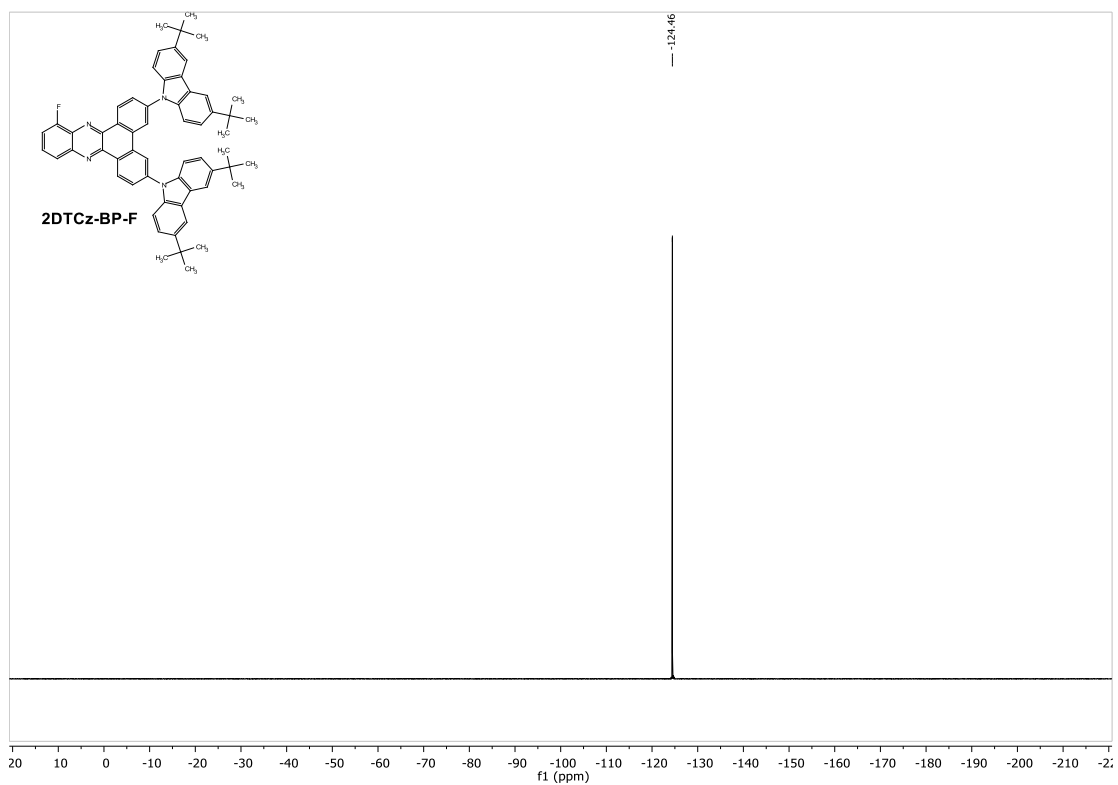


**Figure S3.**  $^{19}\text{F}$  NMR – 2DTCz-BP-F, 376 MHz,  $\text{CDCl}_3$ .

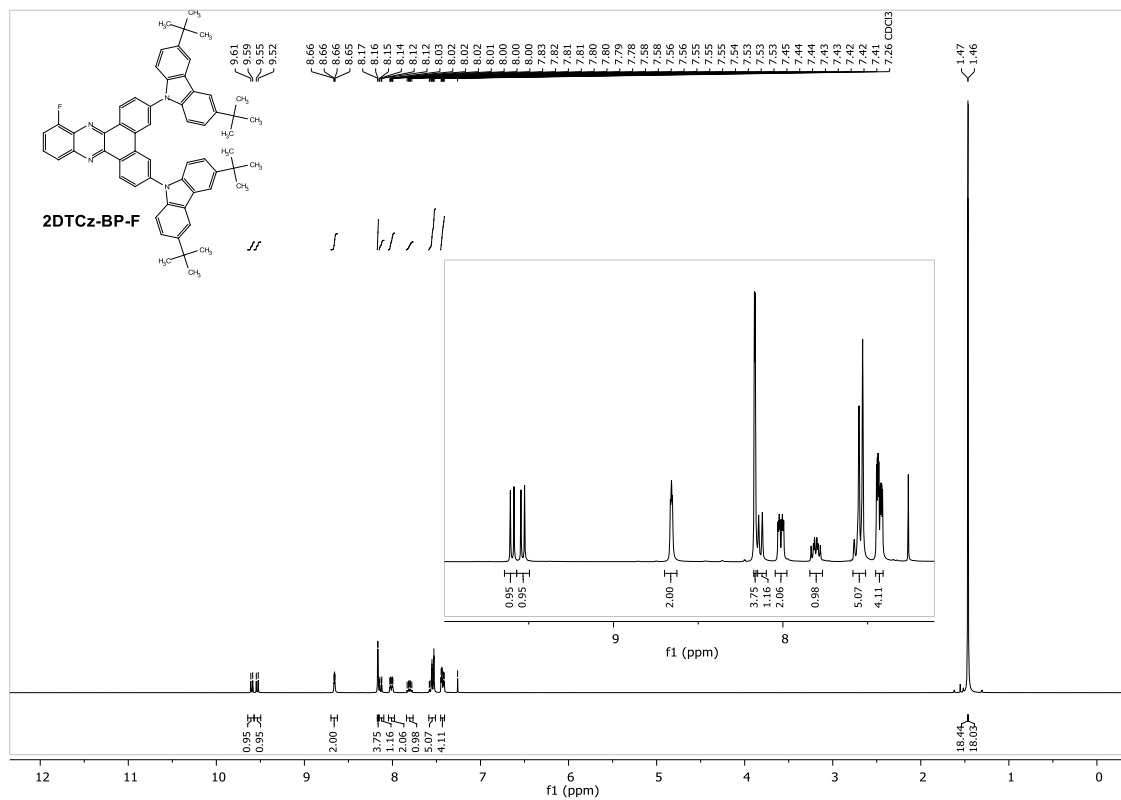


**Figure S4.**  $^1\text{H}$  NMR – 2DTCz-BP-F, 400 MHz,  $\text{CDCl}_3$ .

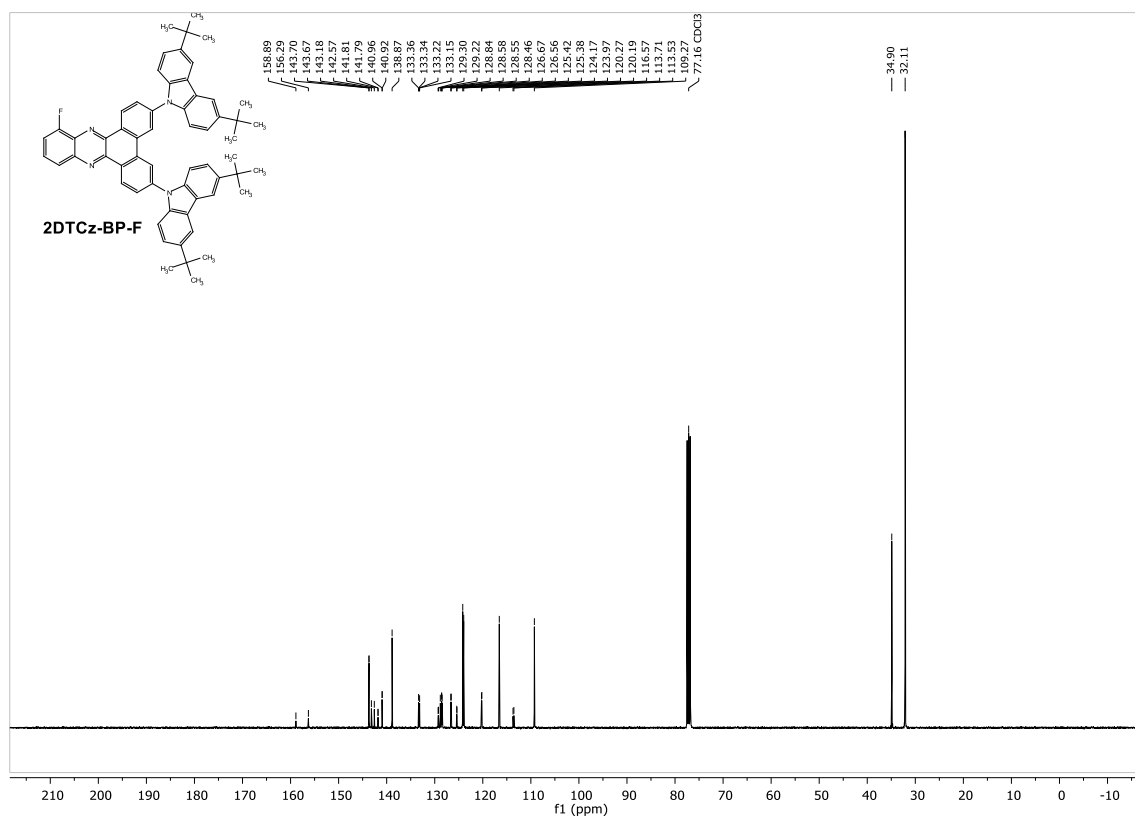


**Figure S5.** <sup>13</sup>C NMR – 2DTCz-BP-F, 101 MHz, CDCl<sub>3</sub>.

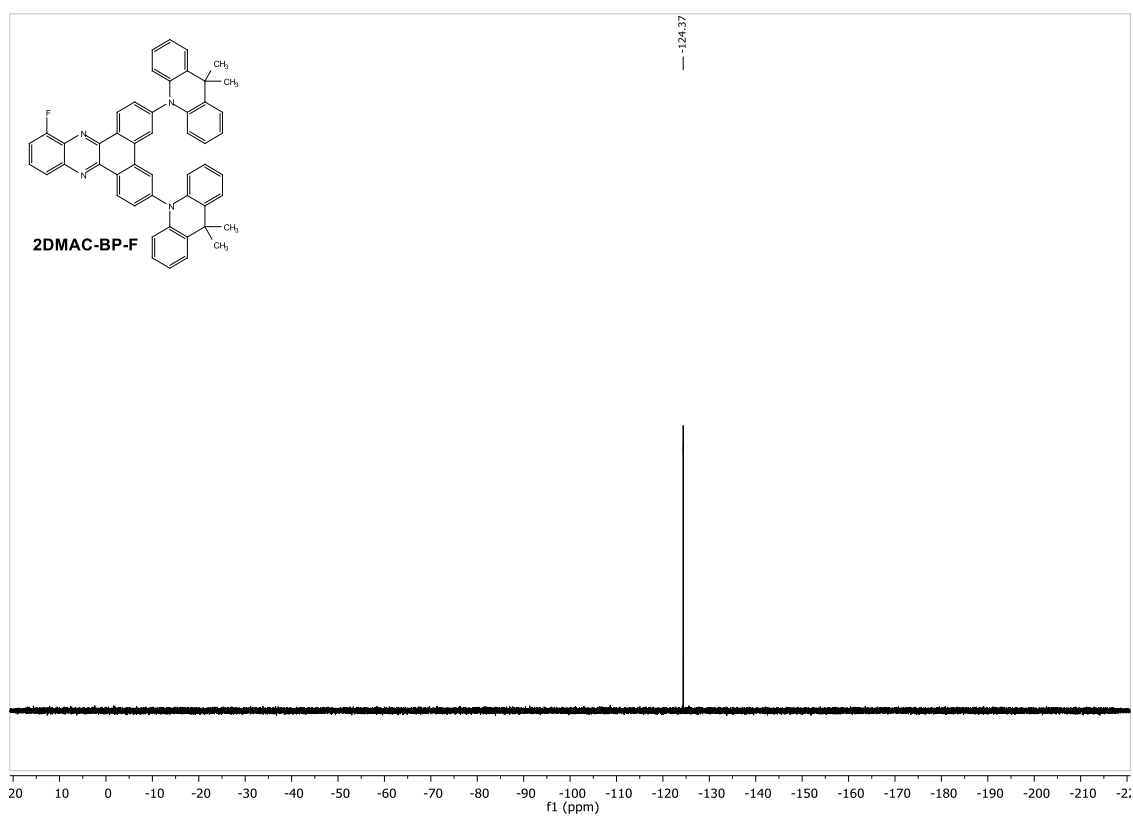


**Figure S6.** <sup>19</sup>F NMR - 2DMAC-BP-F, 376 MHz, CDCl<sub>3</sub>.

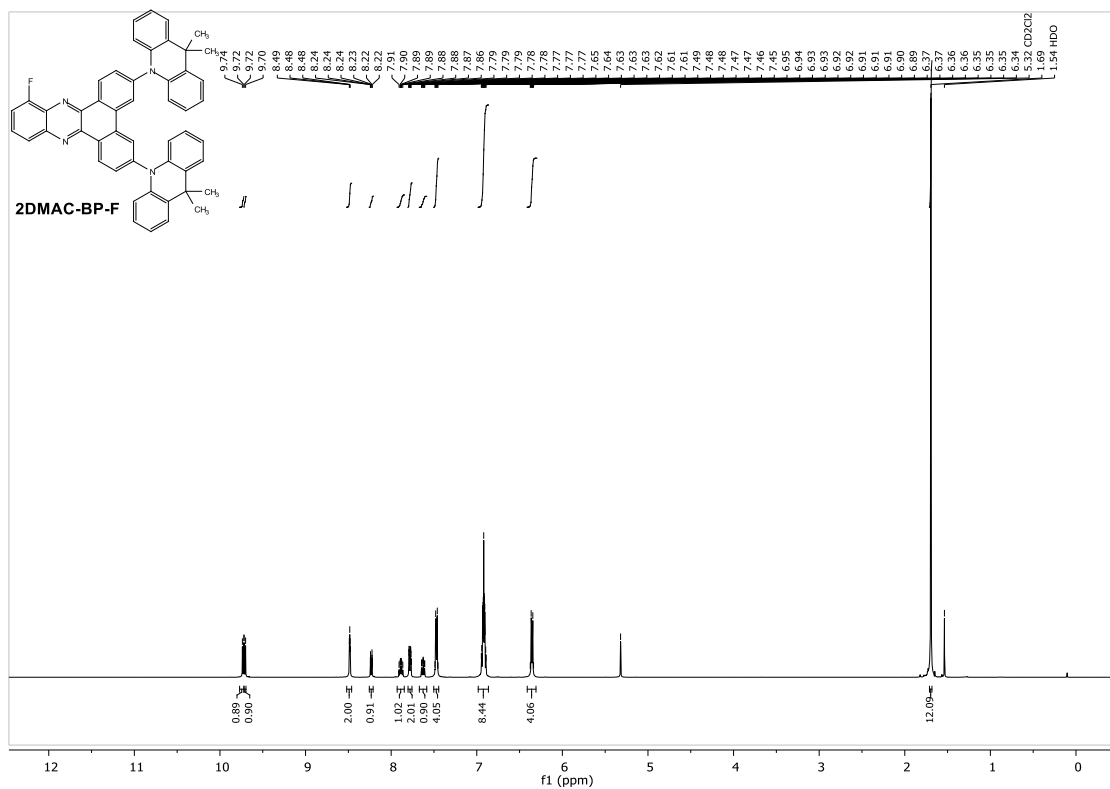


**Figure S7.**  $^1\text{H}$  NMR – 2DMAC-BP-F, 500 MHz,  $\text{CD}_2\text{Cl}_2$ .

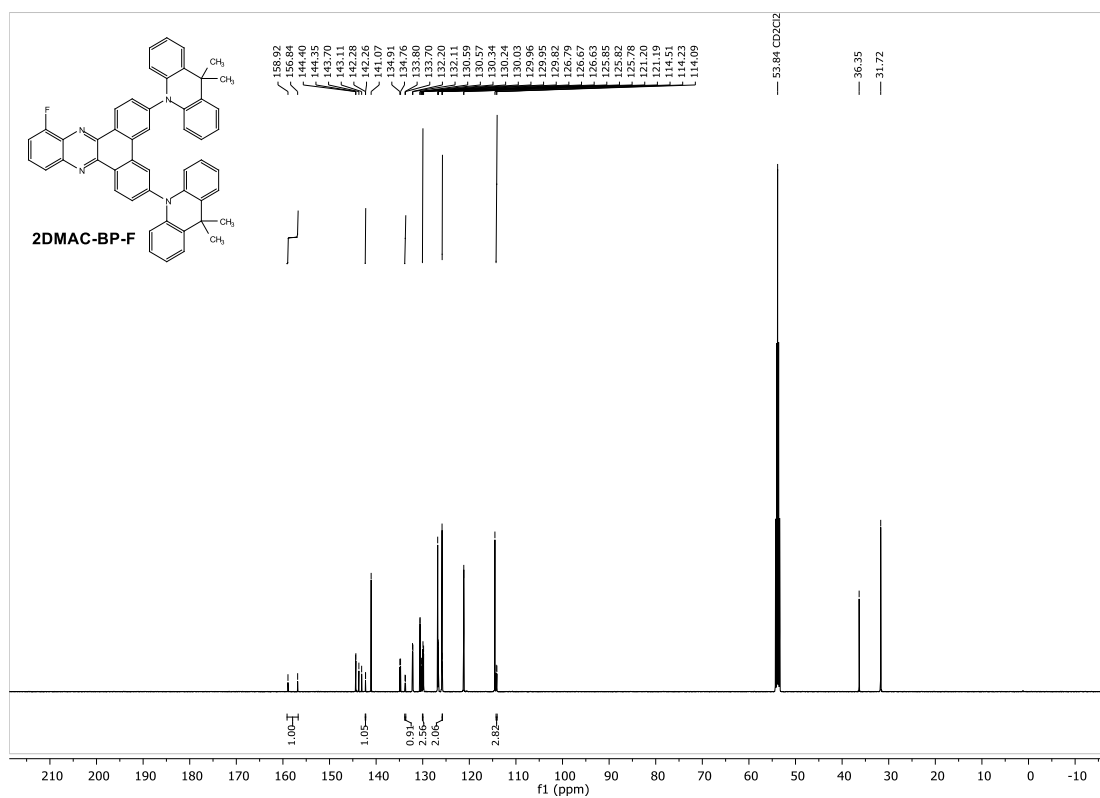


**Figure S8.**  $^{13}\text{C}$  NMR – 2DMAC-BP-F, 126 MHz,  $\text{CD}_2\text{Cl}_2$ .

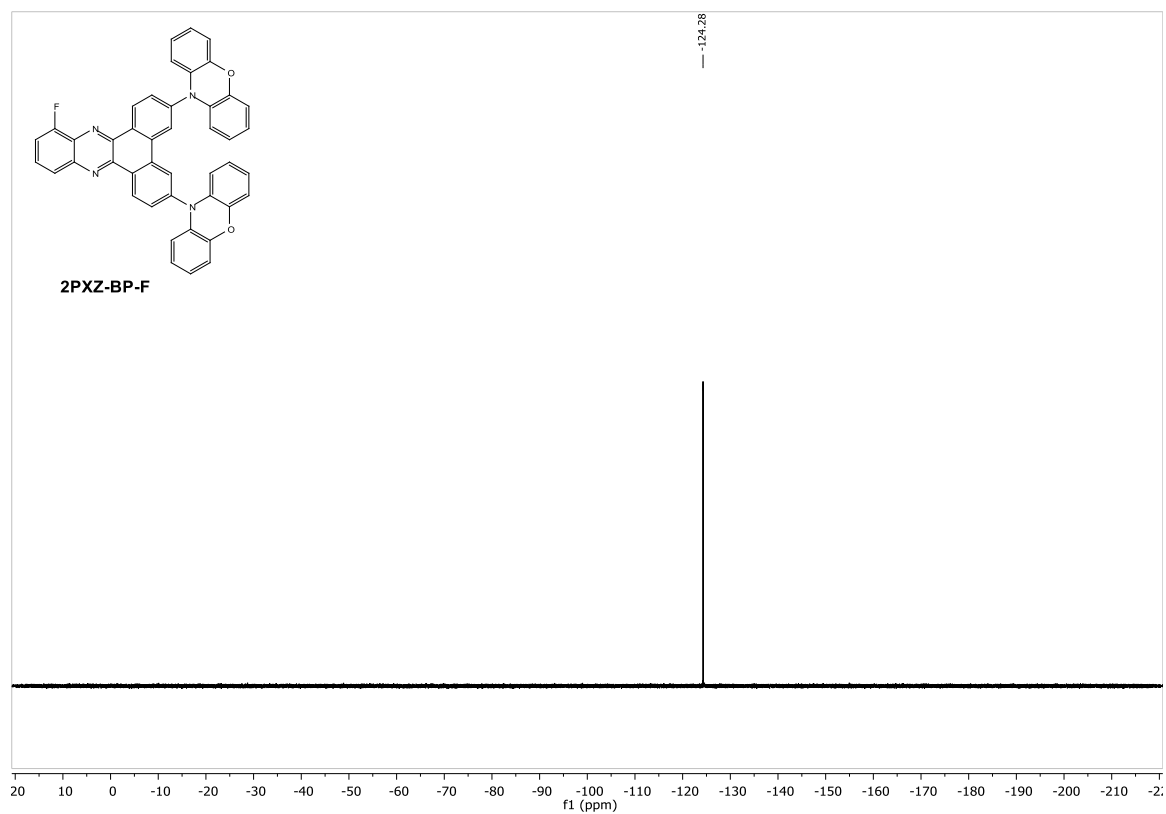


**Figure S9.**  $^{19}\text{F}$  NMR - 2PXZ-BP-F, 376 MHz,  $\text{CDCl}_3$ .

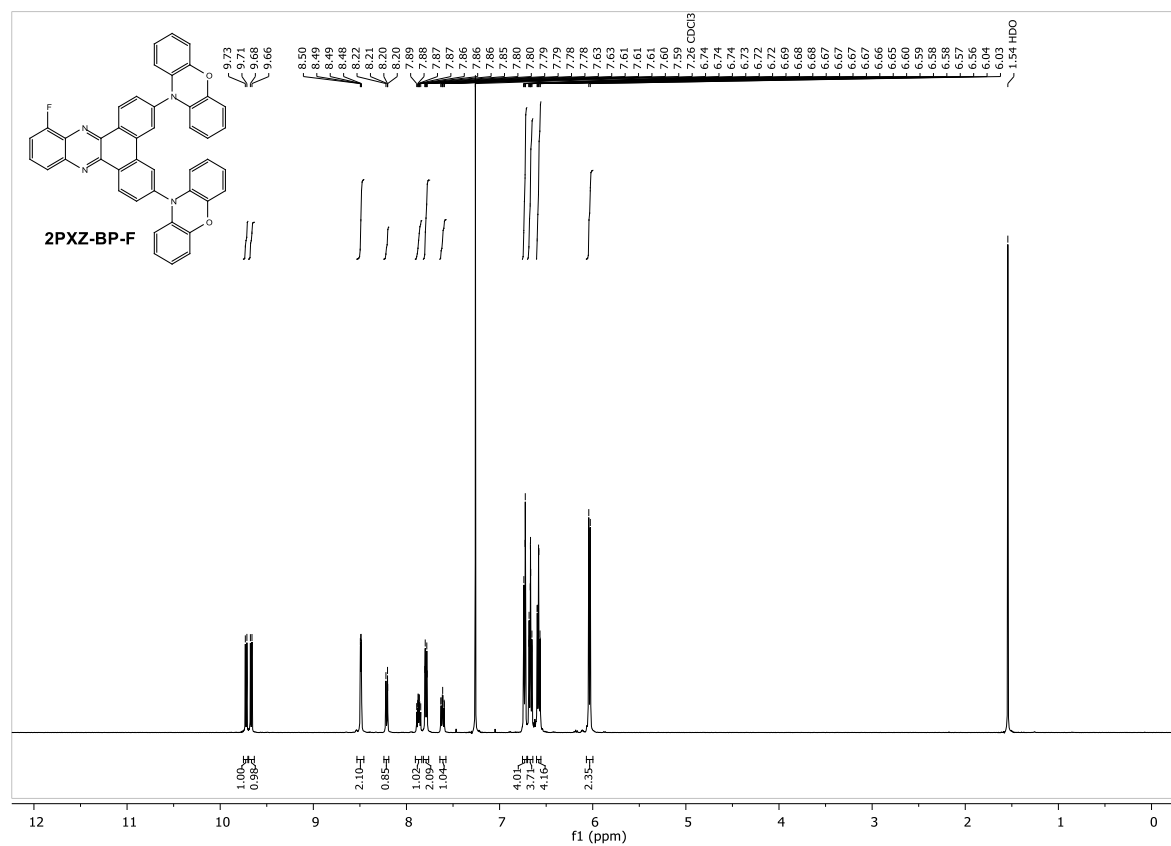


**Figure S10.**  $^1\text{H}$  NMR – 2PXZ-BP-F, 500 MHz,  $\text{CDCl}_3$ .

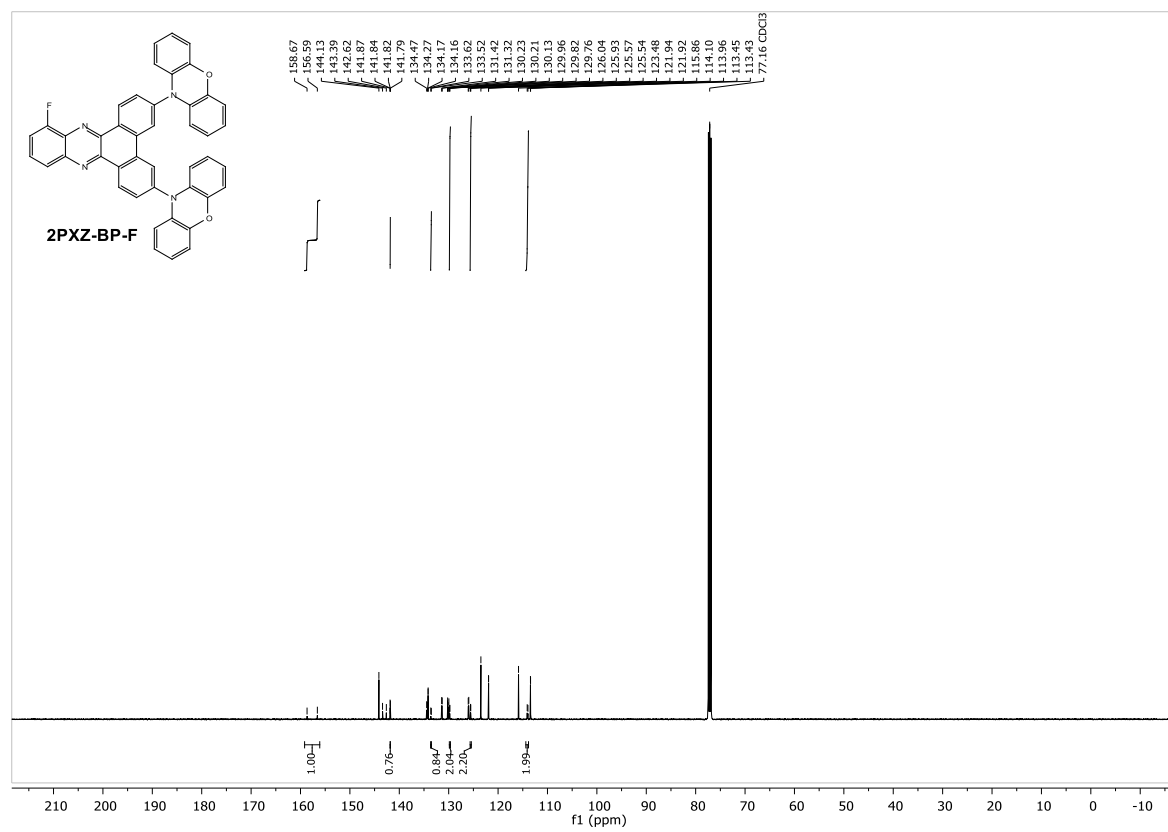


**Figure S11.**  $^{13}\text{C}$  NMR – **2PXZ-BP-F**, 126 MHz,  $\text{CDCl}_3$ .

### 3. Crystal Structure Determinations

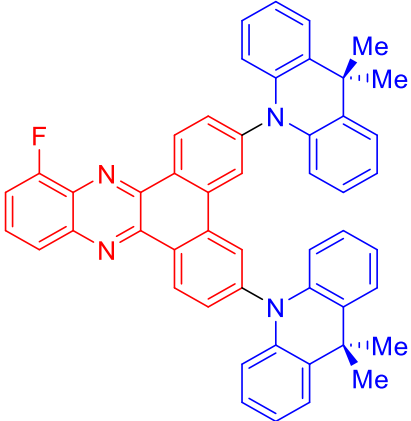
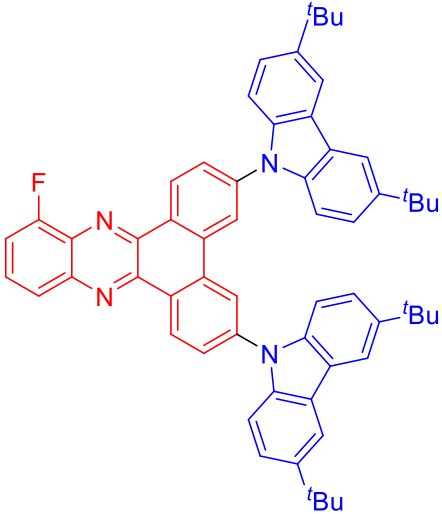
The single-crystal X-ray diffraction study was carried out on a Bruker D8 Venture diffractometer with a PhotonII detector at 298(2) K or 173(2) K using Cu-K $\alpha$  radiation ( $\lambda = 1.54178 \text{ \AA}$ ). Dual space methods (SHELXT)<sup>10</sup> were used for structure solution, and refinement was carried out using SHELXL-2014 (full-matrix least-squares on  $F^2$ )<sup>11</sup>. Hydrogen atoms were refined using a riding model. Semi-empirical absorption corrections were applied. **2DMAC-BP-F** is refined as an inversion twin. In **2DMAC-BP-F**, the F-atom is disordered about a mirror plane. In **2DTCz-BP-F** are 4 crystallographic independent molecules in the asymmetric unit. In each molecule, the F-atoms are disordered (about a mirror plane). In 2 voids are 20 benzene solvent molecules per void; due to the bad quality of the data of **2DTCz-BP-F**, the data were not deposited with The Cambridge Crystallographic Data Centre.

**2DMAC-BP-F (sb1439\_hy)**: red crystals,  $\text{C}_{50}\text{H}_{37}\text{FN}_4 \cdot 2(\text{CH}_2\text{Cl}_2)$ ,  $M_r = 882.69$ , crystal size  $0.36 \times 0.12 \times 0.06 \text{ mm}$ , orthorhombic, space group  $Pmn2_1$  (No. 31),  $a = 16.2097(7) \text{ \AA}$ ,  $b = 7.3687(3) \text{ \AA}$ ,  $c = 18.0747(7) \text{ \AA}$ ,  $V = 2158.92(15) \text{ \AA}^3$ ,  $Z = 2$ ,  $\rho = 1.358 \text{ Mg/m}^3$ ,  $\mu(\text{Cu-K}\alpha) = 2.86 \text{ mm}^{-1}$ ,  $F(000) = 916$ ,  $T = 298 \text{ K}$ ,  $2\theta_{\text{max}} = 145.2^\circ$ , 38535 reflections, of which 4395 were independent ( $R_{\text{int}} = 0.034$ ), 290 parameters, 255 restraints (see cif-file for details),  $R_1 = 0.046$  (for 4246  $I > 2\sigma(I)$ ),  $wR_2 = 0.131$  (all data),  $S = 1.08$ , largest diff. peak / hole =  $0.37 / -0.39 \text{ e \AA}^{-3}$ , (BASF =  $0.48(3)$ ).

**2DTCz-BP-F (sb1426\_hy)**: yellow crystals,  $\text{C}_{60}\text{H}_{57}\text{FN}_4 \cdot 2.5(\text{C}_6\text{H}_6)$ ,  $M_r = 1048.36$ , crystal size  $0.20 \times 0.16 \times 0.06 \text{ mm}$ , monoclinic, space group  $P2_1/c$  (No. 14),  $a = 45.2341(15) \text{ \AA}$ ,  $b = 14.5591(5) \text{ \AA}$ ,  $c = 41.0844(14) \text{ \AA}$ ,  $\beta = 113.749(2)^\circ$ ,  $V = 24765.6(15) \text{ \AA}^3$ ,  $Z = 16$ ,  $\rho = 1.125 \text{ Mg/m}^3$ ,  $\mu(\text{Cu-K}\alpha) = 0.52 \text{ mm}^{-1}$ ,  $F(000) = 8944$ ,  $T = 173 \text{ K}$ ,  $2\theta_{\text{max}} = 144.4^\circ$ , 223270 reflections, of which 48596 were independent ( $R_{\text{int}} = 0.036$ ) (38367 with  $I > 2\sigma(I)$ ).

CCDC 2086119 (**2DMAC-BP-F**) contains the supplementary crystallographic data for this paper. These data can be obtained free of charge from The Cambridge Crystallographic Data Centre via [www.ccdc.cam.ac.uk/data\\_request/cif](http://www.ccdc.cam.ac.uk/data_request/cif). Due to the bad quality of the data of **2DTCz-BP-F**, the data were not deposited with The Cambridge Crystallographic Data Centre.

**Table S1.** Calculated mean deviation from the L.S. planes (without H and <sup>t</sup>Bu groups),  $\sigma$ [Å], and dihedral angles,  $\varphi$ , between the normal of the L.S. planes.

	<p><b>2DMAC-BP-F (SB1439)</b> <i>crystallographic C<sub>s</sub> symmetry</i></p> <p>R = 10-fluorodibenzo[<i>a,c</i>]phenazine            B1 = B2 = 9,9-dimethyl-9,10-dihydroacridine</p> <table border="1" data-bbox="671 616 979 853"> <tbody> <tr> <td><math>\sigma</math>(R)</td> <td>0.055Å</td> </tr> <tr> <td><math>\sigma</math>(B1)</td> <td>0.045Å</td> </tr> <tr> <td><math>\sigma</math>(B2)</td> <td>0.045Å</td> </tr> <tr> <td><math>\varphi</math>(R-B1)</td> <td>65°</td> </tr> <tr> <td><math>\varphi</math>(R-B2)</td> <td>65°</td> </tr> <tr> <td><math>\varphi</math>(B1-B2)</td> <td>80°</td> </tr> </tbody> </table>	$\sigma$ (R)	0.055Å	$\sigma$ (B1)	0.045Å	$\sigma$ (B2)	0.045Å	$\varphi$ (R-B1)	65°	$\varphi$ (R-B2)	65°	$\varphi$ (B1-B2)	80°																							
$\sigma$ (R)	0.055Å																																			
$\sigma$ (B1)	0.045Å																																			
$\sigma$ (B2)	0.045Å																																			
$\varphi$ (R-B1)	65°																																			
$\varphi$ (R-B2)	65°																																			
$\varphi$ (B1-B2)	80°																																			
	<p><b>2DTCz-BP-F (SB1426)</b>            Four crystallographic independent molecules</p> <p>R = 10-fluorodibenzo[<i>a,c</i>]phenazine            B1 = B2 = 3,6-di-<i>tert</i>-butyl-9<i>H</i>-carbazole</p> <table border="1" data-bbox="671 1220 1401 1496"> <thead> <tr> <th>SB1426</th> <th>Mol1</th> <th>Mol2</th> <th>Mol3</th> <th>Mol4</th> </tr> </thead> <tbody> <tr> <td><math>\sigma</math>(R)</td> <td>0.054Å</td> <td>0.086Å</td> <td>0.059Å</td> <td>0.088Å</td> </tr> <tr> <td><math>\sigma</math>(B1)</td> <td>0.033Å</td> <td>0.011Å</td> <td>0.023Å</td> <td>0.017Å</td> </tr> <tr> <td><math>\sigma</math>(B2)</td> <td>0.029Å</td> <td>0.023Å</td> <td>0.020Å</td> <td>0.028Å</td> </tr> <tr> <td><math>\varphi</math>(R-B1)</td> <td>49°</td> <td>44°</td> <td>59°</td> <td>42°</td> </tr> <tr> <td><math>\varphi</math>(R-B2)</td> <td>39°</td> <td>49°</td> <td>38°</td> <td>53°</td> </tr> <tr> <td><math>\varphi</math>(B1-B2)</td> <td>67°</td> <td>85°</td> <td>79°</td> <td>86°</td> </tr> </tbody> </table>	SB1426	Mol1	Mol2	Mol3	Mol4	$\sigma$ (R)	0.054Å	0.086Å	0.059Å	0.088Å	$\sigma$ (B1)	0.033Å	0.011Å	0.023Å	0.017Å	$\sigma$ (B2)	0.029Å	0.023Å	0.020Å	0.028Å	$\varphi$ (R-B1)	49°	44°	59°	42°	$\varphi$ (R-B2)	39°	49°	38°	53°	$\varphi$ (B1-B2)	67°	85°	79°	86°
SB1426	Mol1	Mol2	Mol3	Mol4																																
$\sigma$ (R)	0.054Å	0.086Å	0.059Å	0.088Å																																
$\sigma$ (B1)	0.033Å	0.011Å	0.023Å	0.017Å																																
$\sigma$ (B2)	0.029Å	0.023Å	0.020Å	0.028Å																																
$\varphi$ (R-B1)	49°	44°	59°	42°																																
$\varphi$ (R-B2)	39°	49°	38°	53°																																
$\varphi$ (B1-B2)	67°	85°	79°	86°																																

## 4. DFT Calculations

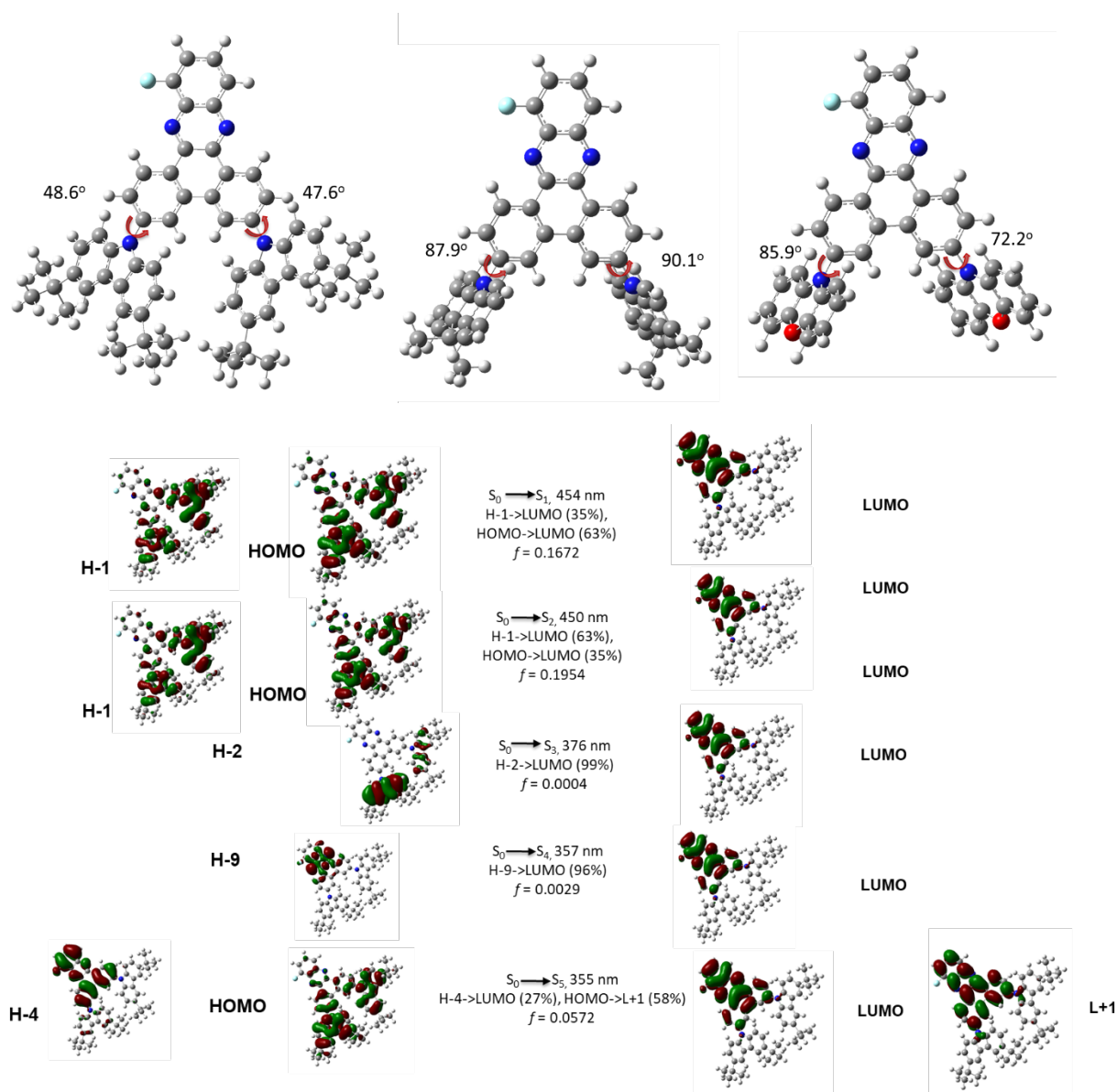


**Figure S12.** Molecular orbitals and the oscillator strength ( $f$ ) of the  $S_0$ - $S_{1-5}$  transition of 2DTCz-BP-F.

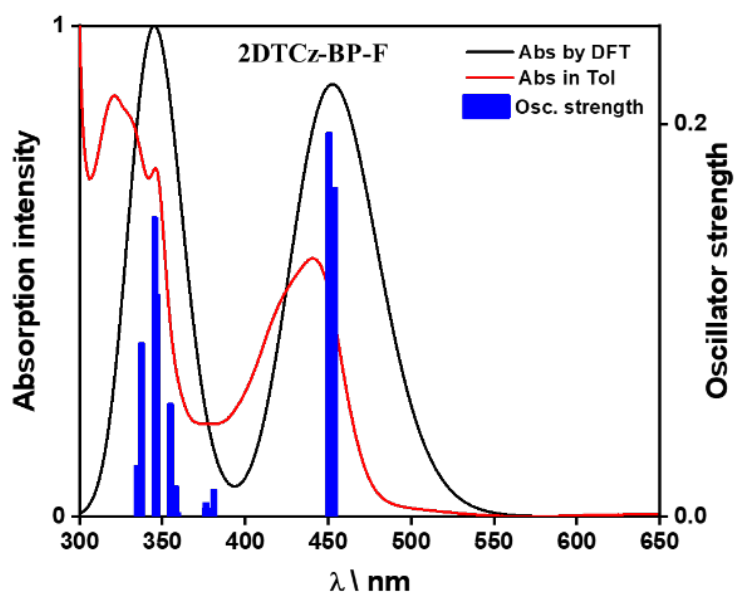


Figure S13. TDA simulation and experimental UV-Vis spectra of 2DTCz-BP-F.

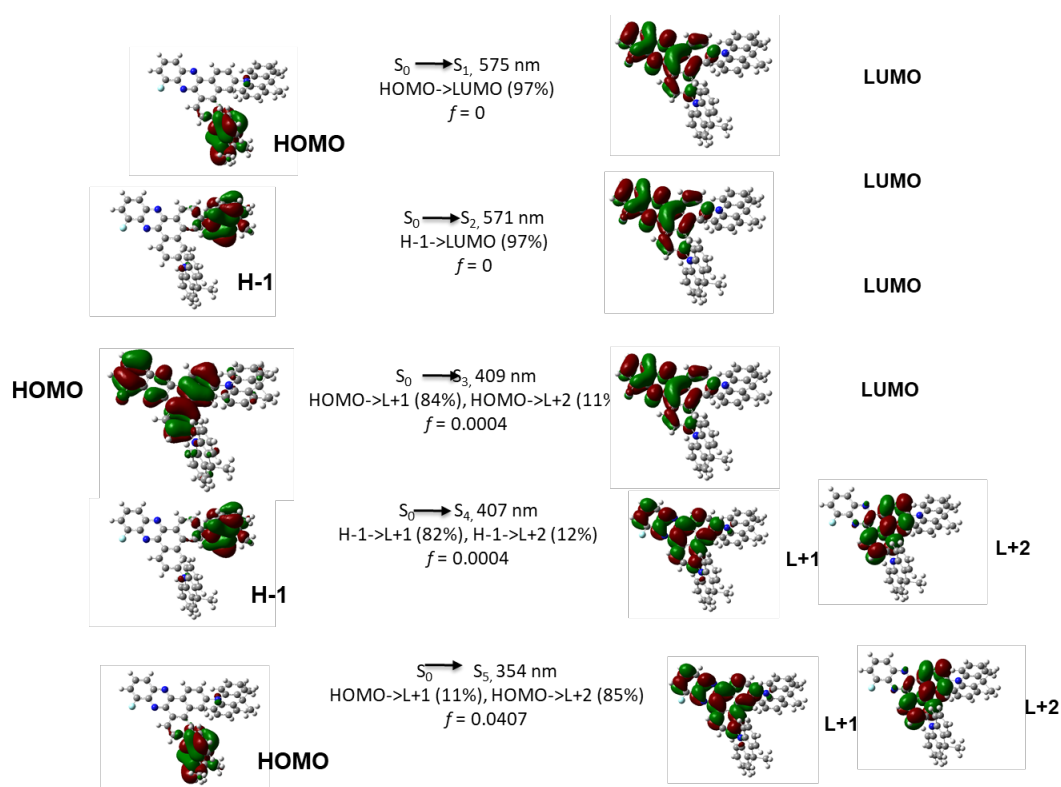


Figure S14. Molecular orbitals and the oscillator strength ( $f$ ) of the  $S_0$ - $S_{1-5}$  transition of 2DMAC-BP-F.

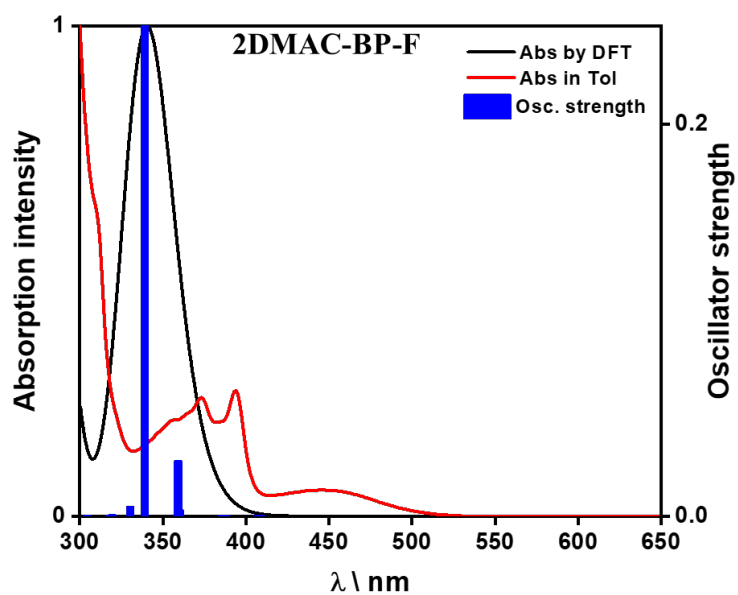


Figure S15. TDA simulation and experimental UV-Vis spectra of 2DMAC-BP-F.

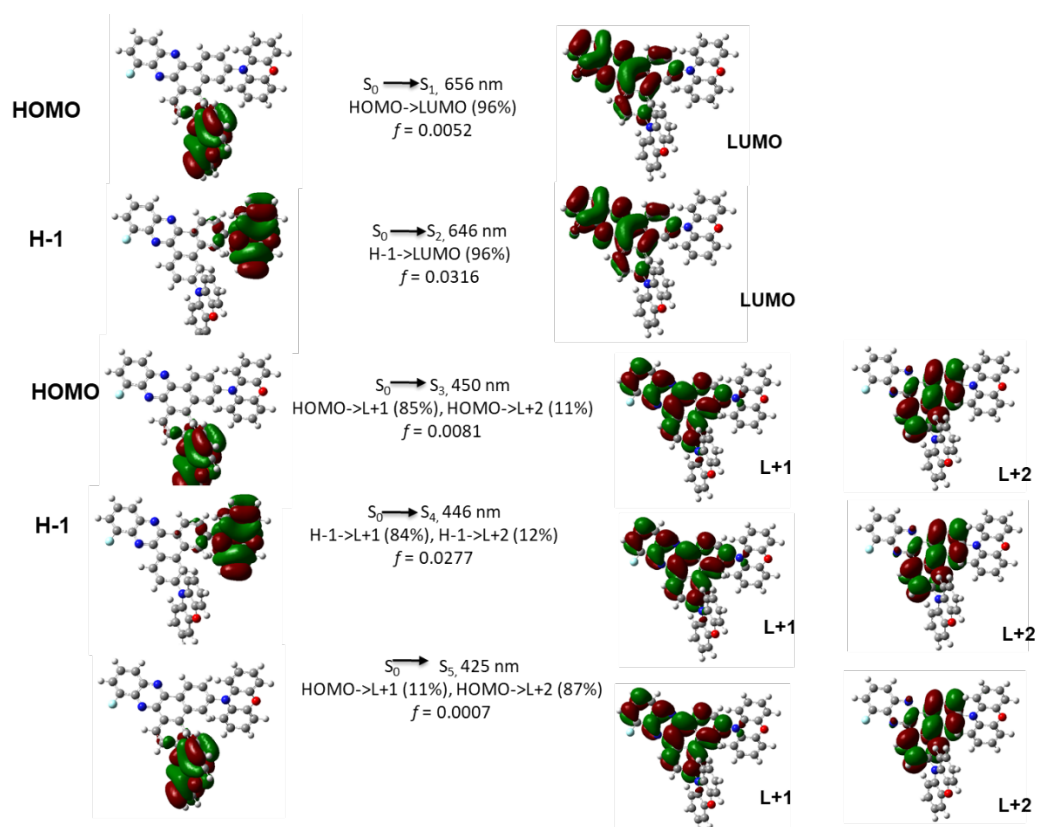
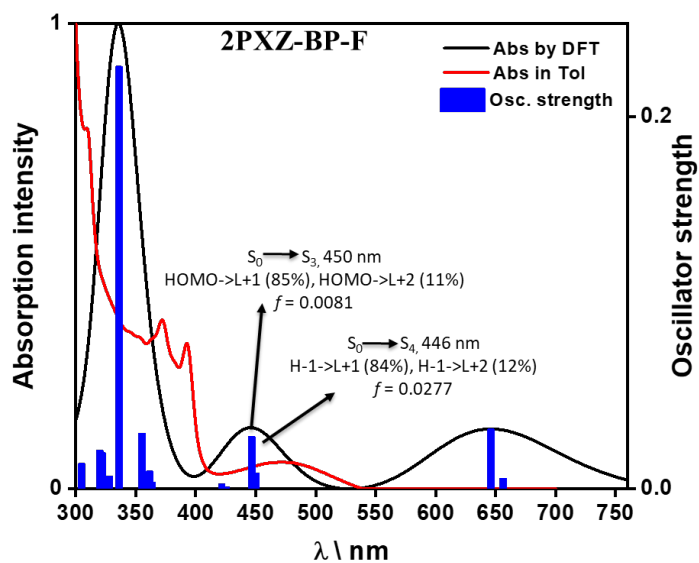


Figure S16. Molecular orbitals and the oscillator strength ( $f$ ) of the  $S_0$ - $S_{1-5}$  transition of 2PXZ-BP-F.



**Figure S 17.** TDA simulation and experimental UV-Vis spectra of **2PXZ-BP-F**.

**Table S2.** Calculated HOMO/LUMO energy level,  $S_1/T_1$  energies, and  $\Delta E_{ST}$  of the three compounds by DFT.

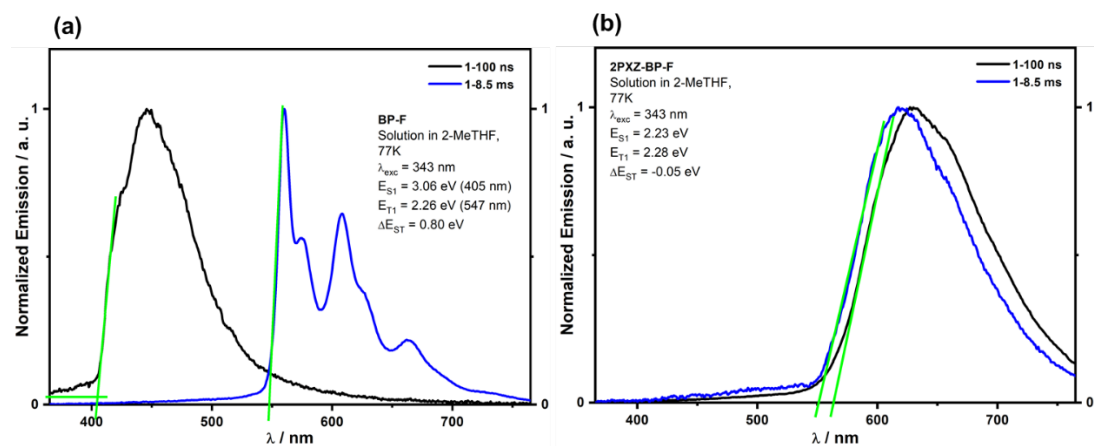
Compound	$E_{HOMO}$ [eV]	$E_{LUMO}$ [eV]	$\Delta E_{H-L}$ [eV]	$S_1$ [eV]	$T_1$ [eV]	$\Delta E_{ST}$ [eV]
<b>2DTCz-BP-F</b>	-5.48	-2.31	3.17	2.73	2.37	0.36
<b>2DMAC-BP-F</b>	-5.18	-2.51	2.67	2.16	2.15	0.01
<b>2PXZ-BP-F</b>	-4.97	-2.58	2.39	1.89	1.87	0.02

## 5. Photophysical Properties

**Table S3.** Summary of solvatochromic PL properties of **2D-BP-F** series.

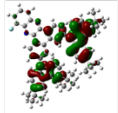
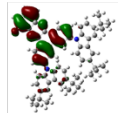
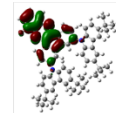
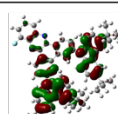
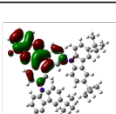
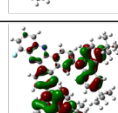
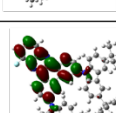
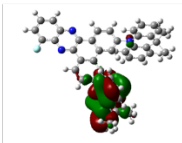
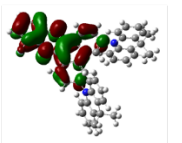
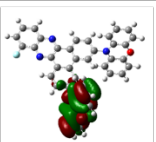
Compound	Solvent	$\lambda_{\text{PL}}^{\text{a}}$ [nm]	FWHM <sup>b</sup> [nm]
<b>2DTCz-BP-F</b>	Hexane	458	42
	Toluene	505	70
	Et <sub>2</sub> O	529	88
	EtOAc	578	119
	DCM	621	138
<b>2DMAC-BP-F</b>	Hexane	512	69
	Toluene	589	105
	Et <sub>2</sub> O	634	132
	EtOAc	715	186
	DCM	761	-
<b>2PXZ-BP-F</b>	Hexane	569	100
	Toluene	674	148
	Et <sub>2</sub> O	716	186
	EtOAc	-	-
	DCM	-	-

<sup>a</sup> Peak value of PL spectra obtained under aerated conditions at 298 K, concentration  $10^{-5}$  M;  $\lambda_{\text{ex}}=343$  nm for **2DTCz-BP-F**,  $\lambda_{\text{ex}}=391$  nm for **2DMAC-BP-F**, and **2PXZ-BP-F**. <sup>b</sup> Full wavelength at half maximum of corresponding PL spectra.



**Figure S18.** Prompt fluorescence and phosphorescence spectra of (a) **BP-F** and (b) **2PXZ-BP-F** in 2-MeTHF at 77 K ( $\lambda_{\text{exc}} = 343$  nm, prompt and delayed fluorescence spectra were obtained in the 1–100 ns and 1–8.5 ms time range, respectively).

**Table S4.** Excitation energy, composition and density plots of dominant molecular orbital transitions of **2DTCz-BP-F**, **2DMAC-BP-F**, and **2PXZ-BP-F** (isovalue = 0.02).

Excited state	Energy /eV	Dominant orbital transition	Corresponding occupied orbital	Corresponding unoccupied orbital
<b>2DTCz-BP-F</b>				
<b>T<sub>1</sub></b>	2.37	HOMO-1 → LUMO (0.39)		
		HOMO-4 → LUMO (0.30)		
		HOMO → LUMO (0.20)		
		HOMO → LUMO+1 (0.03)		
<b>2DMAC-BP-F</b>				
<b>T<sub>1</sub></b>	2.15	HOMO → LUMO (0.96)		
<b>2PXZ-BP-F</b>				
<b>T<sub>1</sub></b>	1.87	HOMO → LUMO (0.97)		

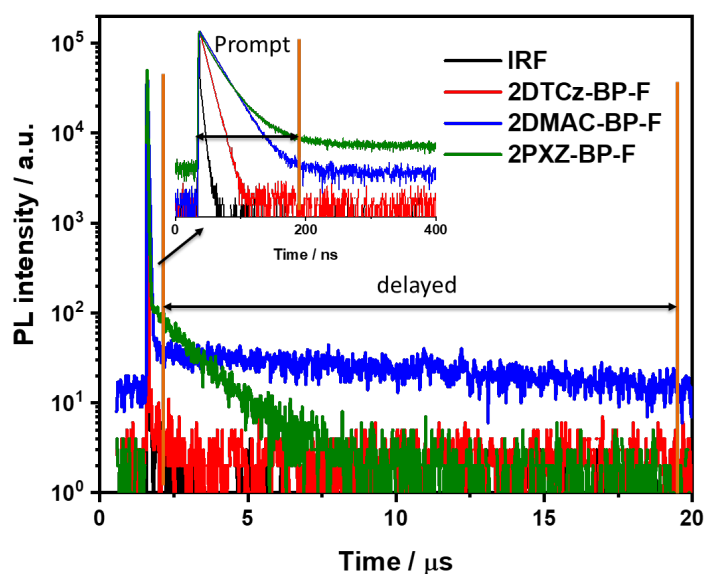


**Figure S19.** Transient PL decay of 2DTCz-BP-F, 2DMAC-BP-F, and 2PXZ-BP-F in degassed toluene. ( $\lambda_{\text{exc}}=379$  nm).

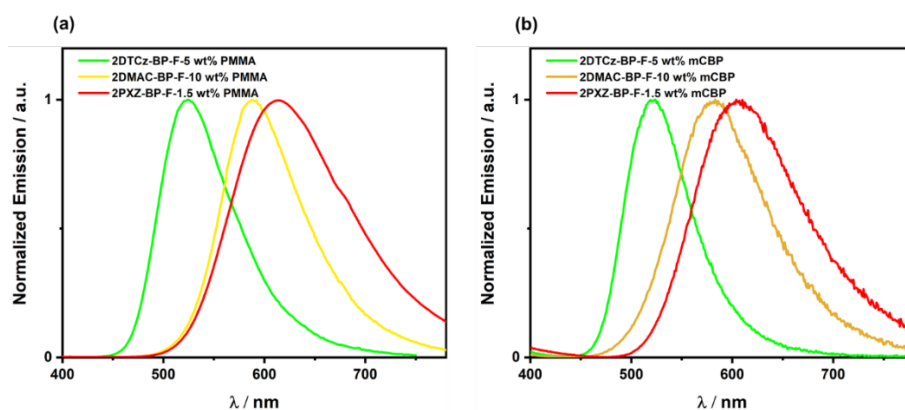


**Figure S20.** PL spectra of 2DTCz-BP-F, 2DMAC-BP-F, and 2PXZ-BP-F in doped film (a) PMMA and (b) mCBP ( $\lambda_{\text{exc}}=343$  nm).

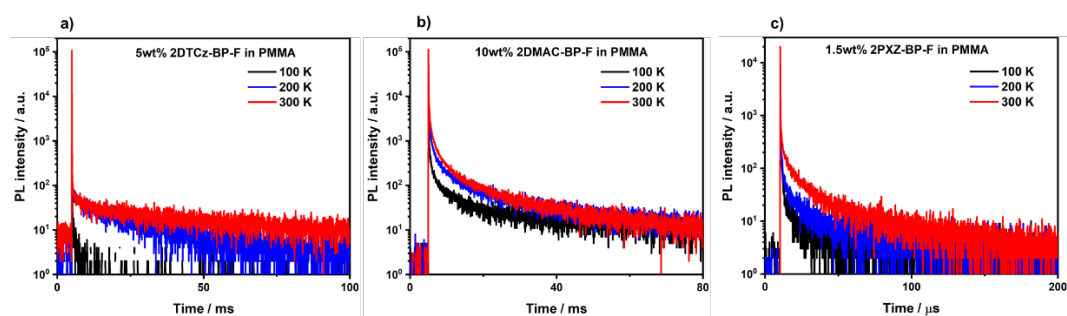


**Figure S21.** Temperature-dependent time-resolved PL decay of a) 5 wt% 2DTCz-BP-F doped PMMA film; b) 10 wt% 2DMAC-BP-F doped PMMA film; c) 1.5 wt% 2PXZ-BP-F doped PMMA ( $\lambda_{\text{exc}}=379$  nm).

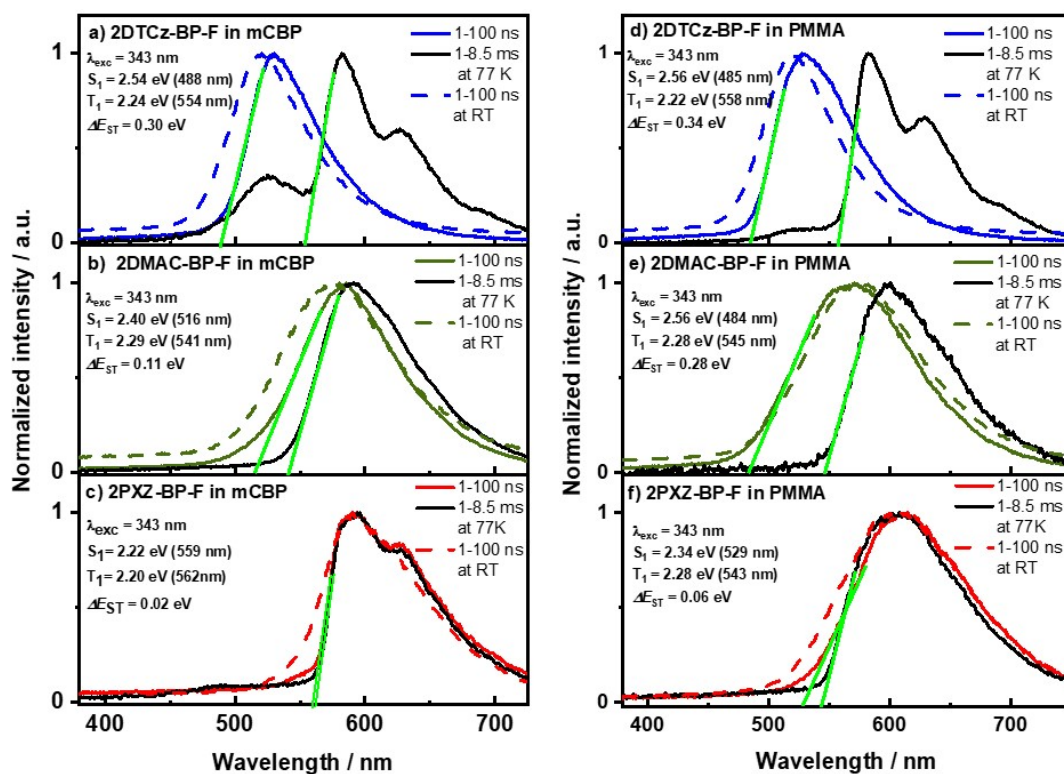


**Figure S22.** Prompt fluorescence and phosphorescence spectra of **2D-BP-F** in doped film at 77 K ( $\lambda_{\text{exc}} = 343$  nm, prompt and delayed fluorescence spectra were obtained in the 1–100 ns and 1–8.5 ms time range, respectively).

**Table S5.** PLQY values ( $\Phi_{\text{PL}}$ ) in solid-state.

Compound	Host	doped ratio	$\Phi_{\text{PL}}$ [%] (in N <sub>2</sub> )	$\Phi_{\text{PL}}$ [%] (in Air)
<b>2DTCz-BP-F</b>	mCBP	1%	50.7	41.0
		5%	59.7	46.8
		10%	53.3	41
<b>2DMAC-BP-F</b>	mCBP	1%	62.2	35.3
		5%	74.3	44.2
		10%	78.0	48.3
<b>2PXZ-BP-F</b>	mCBP	1.5%	58.2	42.3
		3%	50.9	46.6
		5%	42.9	39.9

## 6. OLED Fabrication and Characterization

The OLED devices were fabricated in a bottom emitting architecture via vacuum sublimation in a high vacuum at a base pressure of  $<1 \times 10^{-6}$  mbar. A pre-patterned glass substrate coated with indium doped tin oxide (ITO) was washed sequentially by ultrasonication in chloroform, acetone, and isopropanol for 15 minutes and then exposed to oxygen plasma for 6 min to remove all the dust and organics on the ITO surface. The organic layer sequence and the metal cathode were deposited onto pre-cleaned glass substrates coated with indium tin oxide (ITO), with a sheet resistance of around  $30 \Omega/\text{sq}$ . Organic layers were deposited at a rate of  $0.3\text{-}0.6 \text{ \AA}/\text{s}$ , controlled in situ using the quartz crystal monitors. Doping of the emission layers was achieved through co-evaporation of the emitter and host materials. The electron injection layer LiF was deposited at a rate of  $0.05 \text{ \AA}/\text{s}$ , while the Al cathode was deposited at a rate of  $0.5 \text{ \AA}/\text{s}$  through the shadow mask defining the top electrode. The active area of the OLED was  $2 \text{ mm}^2$ , determined by the spatial overlap of the anode and cathode electrodes. All the devices were encapsulated with glass lids and UV epoxy resin inside the inert atmosphere. The luminance-current-voltage characteristics were measured in an ambient environment using a Keithley 2400 source meter combined with a homemade photodiode connected to a multimeter (Keithley 2000) for the voltage reading. The external quantum efficiency was calculated assuming Lambertian emission distribution. The electroluminescence spectra were recorded by an Andor DV420-BV CCD spectrometer.

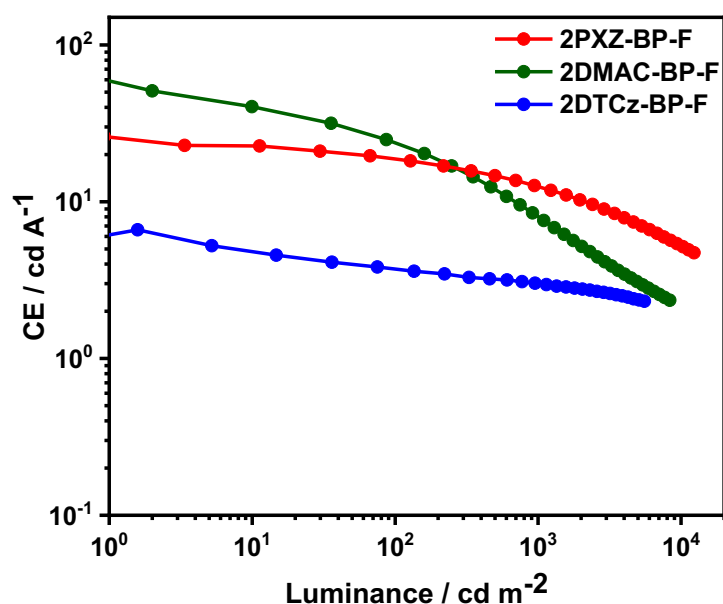


**Figure S23.** Current efficiency versus luminance curves for devices of **2PXZ-BP-F** (1.5 wt%), **2DMAC-BP-F** (10.0 wt%), and **2DTCz-BP-F** (5 wt%) emitters in mCBP host fabricated by thermal evaporation. Device stack; ITO/HATCN (5 nm)/NPB (40 nm)/TCTA (10 nm)/emissive

layer (20 nm)/TmPyPB (40 nm)/LiF (0.6 nm)/Al (100 nm).

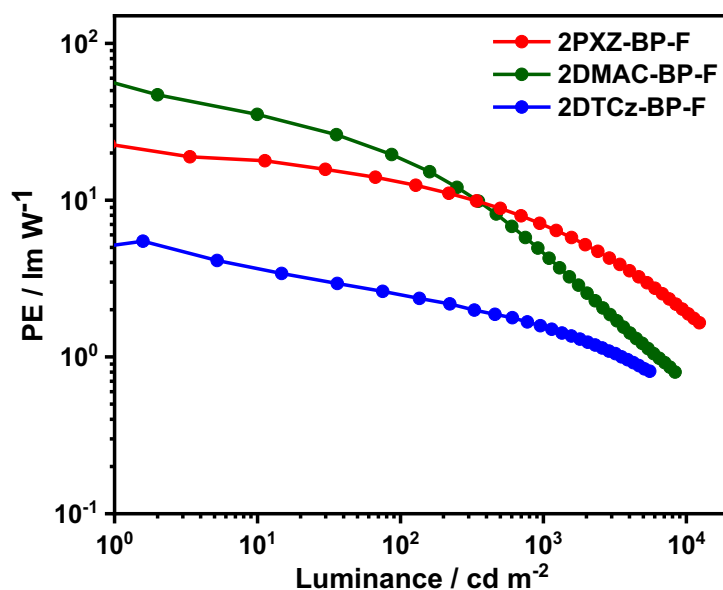


**Figure S24.** Power efficiency versus luminance curves for devices of **2PXZ-BP-F** (1.5 wt%), **2DMAC-BP-F** (10.0 wt%), and **FBP-2DTC** (5 wt%) emitters in mCBP host fabricated by thermal evaporation. Device stack; ITO/HATCN (5 nm)/NPB (40 nm)/TCTA (10 nm)/emissive layer (20 nm)/TmPyPB (40 nm)/LiF (0.6 nm)/Al (100 nm).

#### **OLEDs fabricated with MoO<sub>3</sub> used as HIL.**

We also fabricated OLEDs with **2PXZ-BP-F** and **2DMAC-BP-F** but replaced the HATCN with molybdenum oxide (MoO<sub>3</sub>) [device stack; ITO/ MoO<sub>3</sub> (5 nm)/NPB (40 nm)/TCTA (10 nm)/emissive layer (20 nm)/ TmPyPB (40 nm)/LiF (0.6 nm)/Al (100 nm)]. The current density of **2DMAC-BP-F** and **2PXZ-BP-F** based devices at 9 V is 107.2 mA/cm<sup>2</sup> and 47.7 mA/cm<sup>2</sup>, respectively, when MoO<sub>3</sub> was used as the HIL in both devices. This is very low in comparison to devices which used HATCN as HIL, where the current density of the **2DMAC-BP-F** based device amounts to 313.0 mA/cm<sup>2</sup> and **2PXZ-BP-F** based device is 261.7 mA/cm<sup>2</sup> (**Error! Reference source not found.S5**, Figure 7 and Figure S23). The brightness of the devices is affected proportionally due to the low current density. The maximum brightness of the OLEDs that used MoO<sub>3</sub> as HIL reached up to 3,857 cd/m<sup>2</sup> for **2DMAC-BP-F**, and 3,324 cd/m<sup>2</sup> for **2PXZ-BP-F** based device at 9 V (Figure S23). However, OLEDs which used HATCN as a HIL show brightness up to 7,678 cd/m<sup>2</sup> for **2DMAC-BP-F**, and 12,349 cd/m<sup>2</sup> for **2PXZ-BP-F**. These results indicate that better hole injection materials such as HATCN could be useful to get balanced transport of charge carriers which is important to obtain highly efficient bright TADF OLEDs.

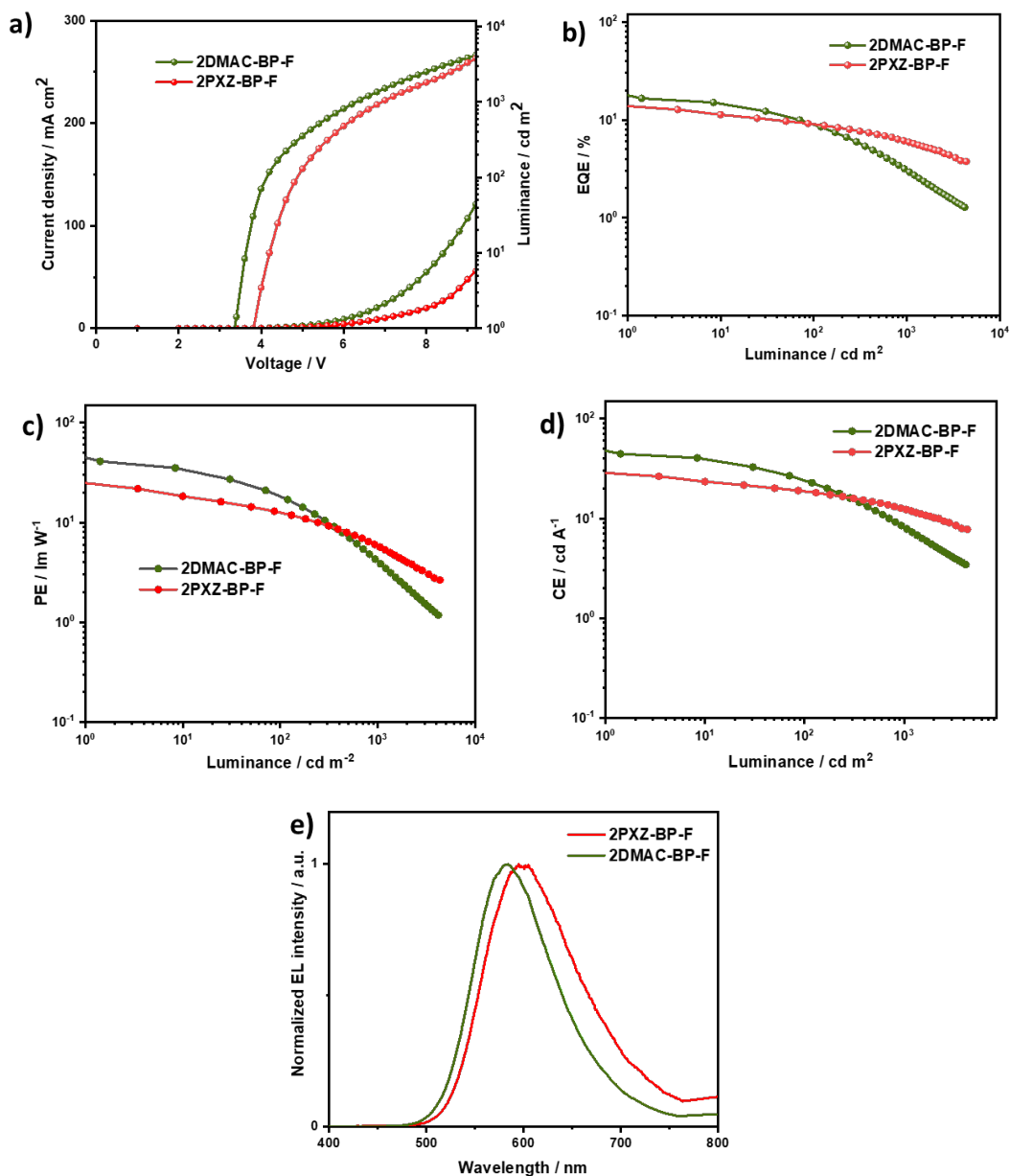


**Figure S25.** OLEDs data of device stack: ITO/MoO<sub>3</sub> (5 nm)/NPB (40 nm)/TCTA (10 nm)/emissive layer (20 nm); mCBP: 1.5 wt% **2PXZ-BP-F** or mCBP: 10 wt% **2DMAC-BP-F**/TmPyPB (40 nm)/LiF (0.6 nm)/Al (100 nm) (a) Current density and luminance *versus* voltage characteristics; (b) External quantum efficiency versus luminance curves; (c) Current efficiency versus luminance curves; (d) Power efficiency versus luminance curves; (e) Electroluminescence spectra of the devices.

**Table S6.** Electroluminescence data for the devices using MoO<sub>3</sub> as HIL.<sup>a</sup>

Emitter	Host	V <sub>on</sub> <sup>b</sup> / V	λ <sub>EL</sub> <sup>c</sup> nm	CE <sup>d</sup> / cd A <sup>-1</sup>	PE <sub>max</sub> / lm W <sup>-1</sup>	EQE <sup>d</sup> / %	CIE <sup>c</sup> / x, y
<b>2PXZ-BP-F</b>	mCBP (1.5%)	3.4	603	28.6/18.7/12.6	24.3	13.9/9.0/6.3	0.550, 0.445
<b>2DMAC-BP-F</b>	mCBP (10%)	3.8	584	47.1/24.2/8.4	43.7	17.8/8.9/3.0	0.514, 0.479

<sup>a</sup>Device stacks; ITO/MoO<sub>3</sub> (5 nm)/NPB (40 nm)/TCTA (10 nm)/emissive layer (20 nm)/TmPyPB (40 nm)/LiF (0.6 nm)/Al (100 nm). <sup>b</sup>The turn-on voltage at a brightness 1 cd m<sup>-2</sup>. <sup>c</sup>The electroluminescence maximum and CIE coordinates recorded at 5 V. <sup>d</sup>The order of measured value: the maximum, then values at 100 and 1000 cd m<sup>-2</sup>.

## 7. References

1. M. J. Frisch, G. W. Trucks, H. B. Schlegel, G. E. Scuseria, M. A. Robb, J. R. Cheeseman, G.; Scalmani, V. Barone, B. Mennucci, G. A. Petersson, H. Nakatsuji, M. Caricato, X. Li, H. P.; Hratchian, A. F. Izmaylov, J. Bloino, G. Zheng, J. L. Sonnenberg, M. Hada, M. Ehara, K. Toyota, R.; Fukuda, J. Hasegawa, M. Ishida, T. Nakajima, Y. Honda, O. Kitao, H. Nakai, T. Vreven, J. A.; Montgomery Jr., J. E. Peralta, F. Ogliaro, M. Bearpark, J. J. Heyd, E. Brothers, K. N. Kudin, V. N.; Staroverov, R. Kobayashi, J. Normand, K. Raghavachari, A. Rendell, J. C. Burant, S. S. Iyengar, J.; Tomasi, M. Cossi, N. Rega, J. M. Millam, M. Klene, J. E. Knox, J. B. Cross, V. Bakken, C. A.; J. Jaramillo, R. Gomperts, R. E. Stratmann, O. Yazyev, A. J. Austin, R. Cammi, C. Pomelli, J. W.; Ochterski, R. L. Martin, K. Morokuma, V. G. Zakrzewski, G. A. Voth, P. Salvador, J. J.; Dannenberg, S. Dapprich, A. D. Daniels, Ö. Farkas, J. B. Foresman, J. V. Ortiz, J. Cioslowski, D. J. Fox. *Gaussian, Inc., Wallingford CT, 2010*.
2. C. Adamo and V. Barone, *J. Chem. Phys.*, 1999, **110**, 6158–6170.
3. S. Grimme, *Chem. Phys. Lett.*, 1996, **259**, 128–137.
4. S. Hirata and M. Head-Gordon, *Chem. Phys. Lett.*, 1999, **314**, 291–299.
5. J. N. Demas and G. A. Crosby, *J. Phys. Chem.*, 1971, **75**, 991–1024.
6. S. Fery-Forgues and D. Lavabre, *J. Chem. Educ.*, 1999, **76**.
7. W. H. Melhuish, *J. Phys. Chem.*, 1961, **65**, 229–235.
8. G. Gritzner and J. Kuta, *Pure Appl. Chem.*, 1984, **56**, 461–466.
9. N. G. Connelly and W. E. Geiger, *Chem. Rev.*, 1996, **96**, 877–910.
10. G. M. Sheldrick, *Acta Crystallogr. A Found. Adv.*, 2015, **71**, 3–8.
11. G. M. Sheldrick, *Acta Crystallogr. C Struct. Chem.*, 2015, **71**, 3–8.